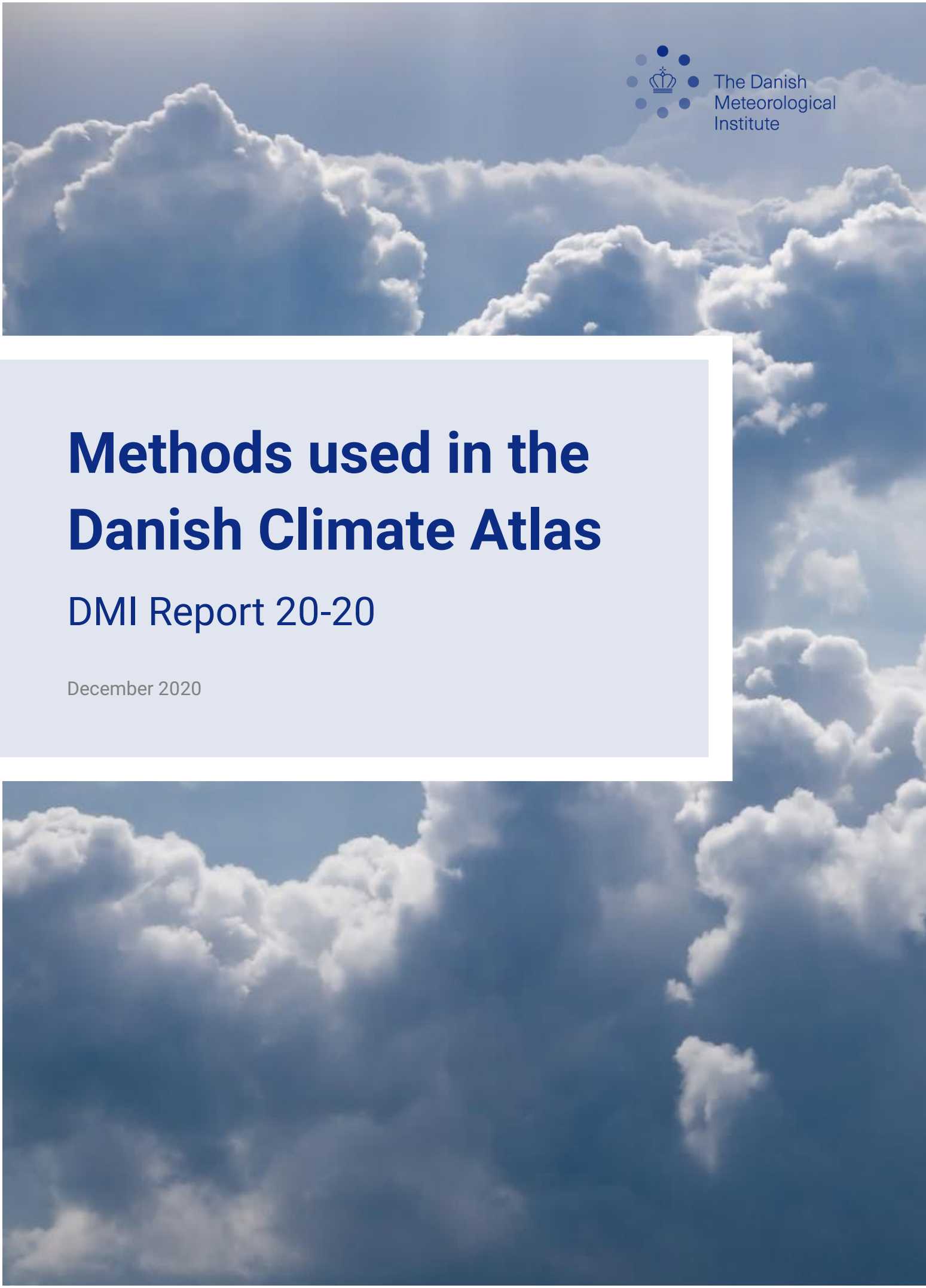

The Danish Meteorological Institute

Methods used in the Danish Climate Atlas

DMI Report 20-20

December 2020

The Danish Meteorological Institute

Title	Methods used in the Danish Climate Atlas
Authors	Peter Thejll, Fredrik Boberg, Torben Schmith, Bo Christiansen, Ole Bøssing Christensen, Marianne Sloth Madsen, Jian Su, Elin Andree, Steffen Olsen, Peter Lang Langen, Kristine Skovgaard Madsen, Rasmus A. Pedersen
Institution	Danish Meteorological Institute
Language	English
Keywords	Climate, Bias correction, Extreme value analysis, sea level, extreme precipitation, storm surge.
Report no.	DMI 20-20
ISBN	978-87-7478-687-0
Version number	1.3
Data version	v2020b
Version date	December 2020
Webpage	`http://www.dmi.dk/klimaatlas`
Copyright	Danish Meteorological Institute

The Danish Meteorological Institute

Contents

Changes in this version

Current report version 1.3., data version v2020b, December 2020.

With the update to version 2020b in December 2020, the Climate Atlas has been expanded with 19 new indicators. The new data presents more details on the future changes in temperature, winds, evaporation, sunshine, frequent and rare storm surges.

Fourteen new atmospheric indicators: Daily high and low temperatures, maximum and minimum temperatures, annual and diurnal temperature intervals, heatwaves (hedebølger og varmebølger), frost days, growing season length, mean wind speed, number of storm events, potential evaporation, and solar radiation.

Five new sea level and storm surge indicators: 100- and 10,000-year storm surge events, 1- and 5-year sea level events, and the change in frequency of current 20-year storm surge events.

The complete overview of the indicators in the current version of Climate Atlas can be found in Table 1.

The main updates to text concern calculation of new temperature indices (in Section 8) and the data for rare storm surge events (in Section 5).

Previous versions:

Version 1.2., data version v2020a, June 2020

This previous version of this report had the DMI number 20-18 and is still available at the DMI index of all reports:
`https://www.dmi.dk/fileadmin/Rapporter/2019/DMIrapport_20_18.pdf`.

Changes compared to version 1.1 / v2019a:
With version v2020a, the Climate Atlas has been updated to include 8 new indicators: the mean number of dry days, the mean duration for the longest dry period, and 5, 20, and 50 year events for hourly and daily precipitation. Furthermore, Climate Atlas is now based on data from more climate models; up to 57 models for daily values and 35 models for hourly values. Data for sea level and storm surges is unchanged since v2019a.

Note that some index numbers have changed since the previous version: the indices for 2, 10, and 100-year events for hourly precipitation are now 151, 153, and 156 (previously 108, 109, and 110), and the indices for 2, 10, and 100-year events for 24-hour precipitation are now 157, 159, and 162 (previously 111, 112, and 113).

Version 1.1., data version v2019a, October 2019

This older version of this report had the DMI number 19-17 and is still available at the DMI index of all reports:
`https://www.dmi.dk/fileadmin/Rapporter/2019/DMIrapport_19_17.pdf`.

1 Introduction

The Danish Climate Atlas provides Danish society with relevant and easy-to-use information on expected future changes in climate, including changes in atmospheric temperatures, precipitation and derived indices, as well as from the sea surrounding Denmark (sea-level and storm surges).

The information is based on observational data and models of the expected climate of the future, taken from EURO-CORDEX archives [Jacob et al., 2014], (`https://euro-cordex.net/`). Such model data are, when taken raw, not expected to correspond closely to reality but must be adjusted or calibrated so that they become more realistic. In this report we describe the applied calibration method together with other processing applied.

The Climate Atlas is available online at

`http://www.dmi.dk/klimaatlas`

and is accompanied with detailed help and user-information. During the planning and calculation period leading up to the release of the Danish Climate Atlas in 2019, thorough reviews of the literature on climate model calibration were carried out, and extensive testing of methods performed. In particular, inter-comparison of methods were performed so that the best methods could be chosen for the Danish Climate Atlas.

It is **the purpose of this Technical Report** to give the necessary details for the methods chosen, and the tests and comparisons that lie behind the choices, as well as to give an overview of the full set of processing leading to the results displayed.

Reading Guide: The report is made up of several sections, and reading each in isolation should be possible. In section 1.1 a sort of 'Executive Summary' is given; section 2 introduces methods used in this report to determine how to best perform so-called model-calibration, and introduces important terminology used throughout the report - the discussion of how we chose our methods may not interest all readers; section 3 is analytical and shows how we determined which method to use in calibrating models in the case these are used for *non-extreme* climate properties; section 4 analyses the same problem, but for use in *extremes* of climate change - precipitation events such as cloudbursts, and sea-level; in sections 5 and 6 methods used for producing projections of future sea levels and storm surges are described; in the online Danish Climate Atlas uncertainties are shown as the 10 and 90 percentiles of the spread due to model choice, in section 7 we discuss issues related to 'uncertainty' in this climate atlas; for each climate index provided we describe in detail the implementation in section 8 - if the reader is only interested in how climate indices were calculated in practise, this is the section to read.

1.1 Brief summary of Climate Atlas contents

The Danish Climate Atlas was launched in 2019, updated twice in 2020, and time-series of climate properties will be made available in 2021.

Currently (December 2020), we provide a total of 44 climate indices (of which 27 are new since the launch in 2019). Eleven is for temperature, 21 for indices describing precipitation, eight are related to the ocean, two for wind, plus solar radiation and potential evaporation. Each index describes absolute values as well as changes in the index, expressed in percent or physical units. Information, except the ocean indices, is available on a 1x1 km grid as well as on an aggregated basis for municipalities and main catchment areas. The ocean indices are available on 34 coastal stretches.

Information will be provided in several data-formats – **.xlsx** spreadsheets, **.netcdf** files and in 'GIS formats'. These data are intended for users requiring download of material for further processing, but the Danish Climate Atlas also provides an online display of the information, with documentation and user guides. Information is made available for the four seasons (and an annual value) for two emission scenarios (RCP4.5 and RCP8.5). Four time periods are used - a present-day reference period (1981-2010) and three future periods (near future 2011-2040, mid-century 2041-2070, and end of century 2071-2100).

The current list of climate indices in the Climate Atlas are listed in Table 1.

Table 1: Summary of climate indices, December 2020.

Index number	Name of index	Notes on implementation
001	Mean temperature	Mean temperature in °C over a year or a season
002	Daily maximum temperature	The mean daily maximum temperature (in °C) seasonally or annually. Describes the highest temperature to be expected on a typical day
003	Daily minimum temperature	The mean daily minimum temperature (°C) seasonally or annually. Describes the lowest temperature to be expected on a typical day
004	Maximum temperature	The maximum temperature (°C) in the season/annually, calculated as the mean of the 30 years' occurrences seasonally/annually
005	Minimum temperature	The minimum temperature (°C) in the season/annually, calculated as the mean of the 30 years' occurrences seasonally/annually

Table 1: Summary of climate indices, December 2020.

Index number	Name of index	Notes on implementation
006	Annual temperature range	Average annual difference between highest and lowest temperature in °C
007	Diurnal temperature range	Seasonal/annual average (in °C) of the range between daily maximum and minimum temperatures
008	Heat-wave days	Number of heat-wave days annually. A 'heat-wave' is indicated when the average of the maximum temperature, over at least three consecutive days, is above 28 °C
009	Warm-wave days	Number of warm-wave days annually. A 'warm-wave' is indicated when the average of the maximum temperature, over at least three consecutive days, is above 25 °C
010	Frost days	Number of days seasonally/annually where the lowest temperature is below freezing (0 °C)
011	Growing season length	The length of the growing season is the number of days between the years' first contiguous 6 days of daily mean temperature above 5 °C to the years last 6-day period of daily mean temperatures above 5 °C
101	Mean precipitation	Mean precipitation in mm/day across a year or a season
102	Max daily precipitation	Sum of precipitation during that day of the year or season when maximum 24-hour precipitation-sum was observed
103	5-day max precipitation	5-day sum of precipitation in that 5-day period of the year or season with largest 5-day sum of precipitation
104	14-day max precipitation	14-day sum of precipitation in that 14-day period of the year or season with largest 14-day sum of precipitation
105	Number of days with over 10 mm precipitation per day	

Table 1: Summary of climate indices, December 2020.

Index number	Name of index	Notes on implementation
106	Number of days with over 20 mm precipitation per day	
107	Number of cloudbursts per year	Number of days with more than 15 mm precipitation in 30 minutes
108	Number of dry days	Number of days of the year or season with precipitation below 1 mm
109	Maximum dry spell length	Length of the longest period of the year or season with consecutive days with precipitation below 1 mm
151	2-year event hourly precipitation	precipitation-sum for one hour that occurs with a return-period of two years
152	5-year event hourly precipitation	precipitation-sum for one hour that occurs with a return-period of five years
153	10-year event hourly precipitation	precipitation-sum for one hour that occurs with a return-period of ten years
154	20-year event hourly precipitation	precipitation-sum for one hour that occurs with a return-period of 20 years
155	50-year event hourly precipitation	precipitation-sum for one hour that occurs with a return-period of 50 years
156	100-year event hourly precipitation	precipitation-sum for one hour that occurs with a return-period of 100 years
157	2-year event in 24-hour precipitation	precipitation-sum over 24 hours that occurs with a return-period of two years
158	5-year event 24-hour precipitation	precipitation-sum over 24 hours that occurs with a return-period of five years
159	10-year event 24-hour precipitation	precipitation-sum over 24 hours that occurs with a return-period of ten years

Table 1: Summary of climate indices, December 2020.

Index number	Name of index	Notes on implementation
160	20-year event 24-hour precipitation	precipitation-sum over 24 hours that occurs with a return-period of 20 years
161	50-year event 24-hour precipitation	precipitation-sum over 24 hours that occurs with a return-period of 50 years
162	100-year event 24-hour precipitation	precipitation-sum over 24 hours that occurs with a return-period of 100 years
201	Mean sea level wrt. coastline	Increase in sea-level, in cm
202	Storm surge 20-year events	Height of storm surge, in cm, of the 20-year event, relative to reference level
203	Storm surge 50-year event	Height of storm surge, in cm, of the 50-year event, relative to reference level
204	Storm surge 100-year event	Height of storm surge, in cm, of the 100-year event, relative to reference level
205	Storm surge 10000-year event	Height of storm surge, in cm, of the 10000-year event, relative to reference level
206	1-year sea level event	Height of the sea level, in cm, of the 1-year event, relative to reference level
208	5-year sea level event	Height of the sea level, in cm, of the 5-year event, relative to reference level
210	Frequency of storm surge 20-year event	Change of the frequency of the storm surge, in number per year, of the 20-year event, relative to reference level
301	Mean wind speed	Average wind speed (in m/s) over a year or a season.
302	Extreme wind	Number of days in a year or season with a maximum wind speed above 25 m/s
401	Solar radiation	Seasonal/annual average of the daily sum of the direct and diffuse radiation from the Sun reaching the (horizontal) surface, in W/m^2

Table 1: Summary of climate indices, December 2020.

Index number	Name of index	Notes on implementation
402	Potential evaporation	The seasonal/annual average potential evaporation (in mm/day) that could evaporate, as given by the Makkink formula

What follows in sections 3, 4, 5 and 6 are detailed studies to determine which calibration methods should be used on model time-series, subsequently used to calculate climate indices describing climate-change – such as future changes in thirty-year means of precipitation or temperature.

This report goes into great technical detail covering the methods behind the Climate Atlas. Note that these details do not concern the *direct use* of the Climate Atlas itself, but is scientific background information written for scientific and expert users.

2 Method overview

Model calibration essentially deals with the reality that distributions of climate model data are not usually identical to distributions of the same quantities observed. The differences can lie in different mean values, or, usually, in distributions that neither have the same mean nor the same shape (widths, for instance). Methods that deal with the task of making model data distributions more or less similar to observed data, are here generally termed ”calibration” methods, with additional nomenclature to indicate precisely which form of adjustment is used. These concepts will be discussed below.

Calibration methods can be quite different, as we shall see, based on which variable considered. Common to them all is that they are based on somehow using information taken from the observational world. An issue arises if the observational data are not very extensive, so each method may have to be adapted to the particulars of the situation.

In climate-change work a ’reference period’ is often employed, such as 1986-2005 (IPCC, AR5), as a baseline to calculate climate change. The beginning and length of this period are typically carefully chosen in order to achieve a number of things. One goal is to help diminish the influence the effect of natural variability – i.e. the reference period should be long enough to smooth out variations, but not so long it extends over important phases of climate change. We have here chosen as ’reference period’ 1981-2010 which is a compromise to have a period as close to present as possible, 30 years long, and to symmetrically overlap the AR5 reference period.

A ’calibration period’ is also chosen, which is the period during which observed and model data both exist. The calibration period is used to determine the data transformations required. This period may be different for different climate variables due to observational constraints.

As is the norm in climate work, statements about future expected climate change are often made in terms of the change between two periods – one will then typically be the reference period while the other is some 'future period' such as 2011-2040, 2041-2070, and 2071-2100 (these will be used in the Climate Atlas, see Figure 2). For example, precipitation-change is quantified in terms of a ratio, while for temperature it is given as a difference.

In this work we shall see two calibration methods evaluated and used. These will be discussed in detail below, but are, in general, the "Bias Correction" methods that transform model data by a comparison of data during the calibration period, and the "δ-change" methods that take expected changes from model data and apply these to observed data. The properties of the calibrated data are therefore different depending on the method used. (See Section 2.2).

It is necessary to test thoroughly which method is best, and the details of this are given in what follows. In general, the testing procedure is based on the 'true world' analogy: model data for present and future periods are collected and one of several models is, in turn, designated 'observations' and a test of performance of various methods that transform the remaining models, one at a time, into those 'observations' is performed. The success of the particular method is evaluated from a closeness measure between the calibrated data and the known 'future observations' in the designated model.

Giving realistic scenarios of future frequencies of occurrence of cloudbursts requires special methods to be applied. This is because models do not represent cloudbursts as such, due to the sub-scale parametrization required: There are precipitation events in model data, of course, but actual realistic cloudbursts are absent (a cloudburst is defined in Denmark as 'at least 15mm of precipitation in half an hour'); this is due to the limited resolution of regional climate models, where convective events are parameterized as opposed to being modelled explicitly. The method chosen is simple but effective - it is based on a scaling between observed cloudburst frequency and hourly model-precipitation frequencies. This choice is based on the assumption that the modelled 1-hour mean-precipitation vs extreme-precipitation relationship does not alter form across time-scales.

Model data are available on a grid – in our case the CORDEX EUR model grid with a spacing between points of $0.11 \times 0.11^\circ$ in a rotated coordinate system (roughly a 12.5$\times$12.5 km grid, in Denmark). Observations are typically available as station series, or as interpolated products. The grid of the observations are typically not the same as used in the models and special considerations have to be made.

First of all, it is important to realise that some climate indices (typically those dealing with extremes) should not be derived from already interpolated data, due to a specific smoothing problem – interpolation does not preserve extremes. Rather, climate indices should be derived at the station level and then an interpolation of that index into a grid-product could be performed. This is not always possible. For instance, particular extreme indices may not have been considered at the time of generating the grid of observational data, and the original observed data may not be easily accessible for re-evaluation.

In addition, the Climate Atlas must deliver information at a resolution level that is useful to the end-users. The grid known as 'det Danske Kvadratnet' [Danmarks Statistik, 2019], which

has a 1x1 km resolution, and is used in the ”Klimagrid Danmark” dataset to be described in section 2.1 below, is used to provide information at high granularity, by interpolation in the CORDEX grid.

The Climate Atlas therefore strives to deliver calibrated data, and then to output several data-formats that address the above expectations.

2.1 Dataset 'Klimagrid Danmark'

The Danish Meteorological Institute operates measurement stations for temperature and precipitation, and other observables, across Denmark. The observational data were used to produce evenly-spaced grids of data (10x10 km for precipitation, and 20x20 km for temperature) called 'Klimagrid Danmark' data ('KGDK' from now on) [Scharling, 1999, 2012, Wang and Scharling, 2012]. The grid used in KGDK is locked to the 'det Danske kvadratnet' grid [Danmarks Statistik, 2019].

Figure 1 shows the locations of the grid-points that make up the precipitation grid (10x10 km) in KGDK.

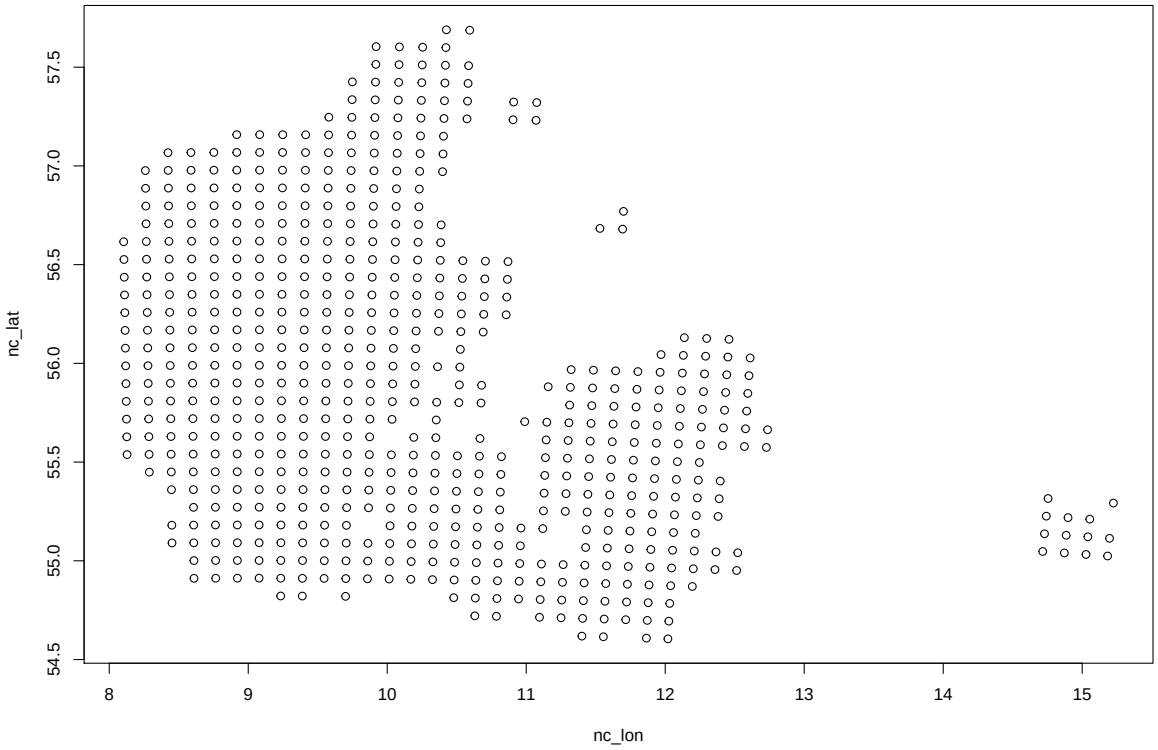

Figure 1: The Klimagrid Danmark grid for precipitation. Note that both Anholt and Læsø are represented.

It should be noted that, in order to match DMI official climate normals for mean precipitation, we are using KGDK precipitation data that are not corrected for undercatch.

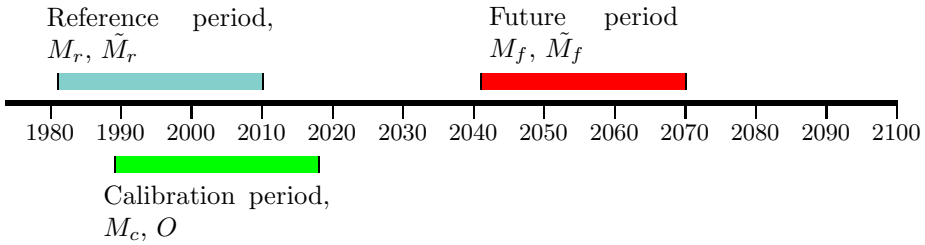

Figure 2: Different time periods used in this work, and nomenclature.

2.2 Nomenclature

Figure 2 explains some of the nomenclature used in this report. A model variable is denoted M. The different periods are indicated with sub-scripts: M_c, M_r, and M_f refer to model values in the calibration period, the reference period, and the future period, respectively. In the calibration period we have simultaneous values of the model M_c and observations O. The calibrated model values in the reference period and the future period are denoted $\tilde{M}_r$, and $\tilde{M}_f$.

There are two over-arching types of calibration methods. The first type is denoted δ-change and is based on a mapping $M_c \to M_f$. This mapping is then applied to O to get $\tilde{M}_f$: $O \to \tilde{M}_f$. The other method is known as bias correction. This is based on a mapping $M_c \to O$ which is then applied to M_f to get $\tilde{M}_f$: $M_f \to \tilde{M}_f$.

In Sections 3 and 4 we will describe a set of calibration methods and test them via cross-validation based on CORDEX models. Based on these tests we will determine the calibration methods to be used in the Danish Climate Atlas. Note that we here are interested in calibration of time-series, and therefore use empirical methods. The study of extremes in precipitation (see section 4) and sea-levels (section 5) uses analytically based methods since a theoretical basis exists for the distribution of extremes.

3 Calibration of time series

3.1 The calibration methods

For both the δ-change and the bias-correction methods a mapping is determined from the calibration period. The mappings will be based on the distributional properties of the time-series, but will be applied to the time-series themselves. However, the mappings we will use are all monotonic. The δ-change method will therefore result in a bias corrected series, $\tilde{M}_f$, that preserves much of the temporal structure of the observations. On the other hand, the bias correction method will result in a series that preserves the main temporal characteristics of the model. This may be important to some users as the temporal characteristics of the model are not always realistic. A draw-back of the δ-change method is that the length of $\tilde{M}_f$ is limited by the length of the calibration period.

For both the δ-change and the bias correction methods a number of mappings can be chosen. The simplest is the additive mean correction. Here the bias correction mapping is given by $\tilde{M}_f = M_c + \overline{O} - \overline{M}_c$. This makes good sense for temperature while for precipitation the multiplicative mean correction $\tilde{M} = M_c\overline{O}/\overline{M}_c$ makes more sense. Overline denotes temporal means.

The mean corrections do not take care of the higher order moments such as the variance. To this end we consider quantile-quantile mappings (*'q-q'* from now on). Let F_O and F_{M_c} be the cumulative distribution functions of observations and the corresponding model variable in the calibration period, respectively. Then $\Xi = F_O^{-1}(F_{M_c})$ is the mapping for the bias correction method and the calibrated values are $\tilde{M}_f = \Xi(M_f)$. Note that the distribution of $\Xi(M_c)$ is per definition identical to the distribution of O. For the δ-change the mapping is $\Xi = F_{M_f}^{-1}(F_{M_c})$ and the calibrated values $\tilde{M}_f = \Xi(O)$.

In particular for the *q-q* mappings there are in practice a number of choices that have to be made. These include the number of quantiles used to represent the cumulative distribution functions (if the lengths of the series are identical then number of quantiles can be the length of the series). Another important choice is the type of extrapolation used for values that fall outside the values of the calibration period (Figure 3). In Figure 4 we show the resulting inclinations for precipitation and temperature for RCP8.5. Evidently, RCP8.5 models are on average wetter (notably winters) and cooler (notably summers) than observations. No inclinations are extremely large, and we expect the method to be robust.

We must also decide if we want to work on daily or monthly values even if only monthly results are needed.

For the precipitation a particular problem arises regarding the treatment of wet days and dry days. After some testing we have chosen the following simple and robust method. We adjust model precipitation series to replicate the fraction of wet days in the calibration period. In the case where the model has more wet days than observation, the days with the lowest

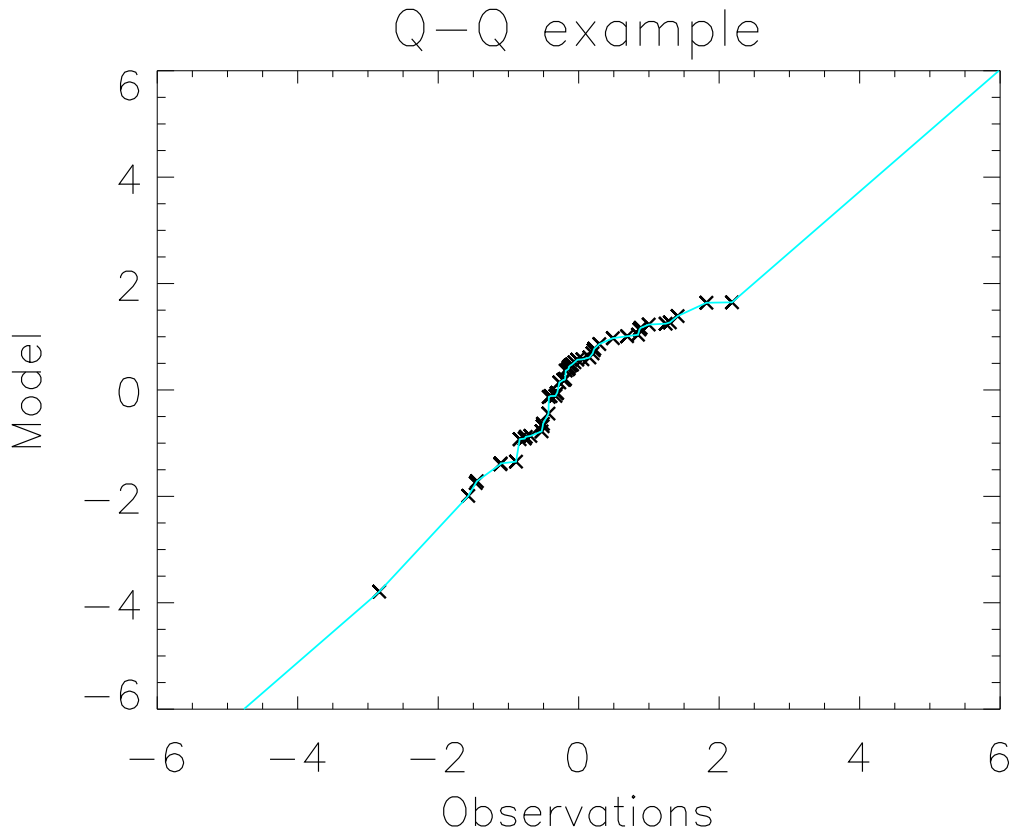

Figure 3: An example of how to extend the *q-q* map into the region without data. Here the last points to each side are extended with a straight line with the slope of the least squares line fitted robustly through all the points.

model precipitation will be converted to dry days. In the opposite case, we promote modelled dry days to wet days by promoting days with the highest sub-threshold precipitation to the threshold precipitation amount; if necessary, random dry days will be similarly promoted.

3.2 Cross-validation

We determine the best methods by cross-validation based on 15 CORDEX models. The models are shown in Table 2 and we have data from historical experiments and the scenarios RCP4.5 and RCP8.5.

In cross-validation a model is chosen to represent the 'truth' (observations). The remaining 14 models are then calibrated against this 'truth'. As data now exist for the 'truth' in the future the calibration method can be validated. The 'truth' can be chosen as each of the 15 models and this gives us 15*14 different combinations of 'truth'/model.

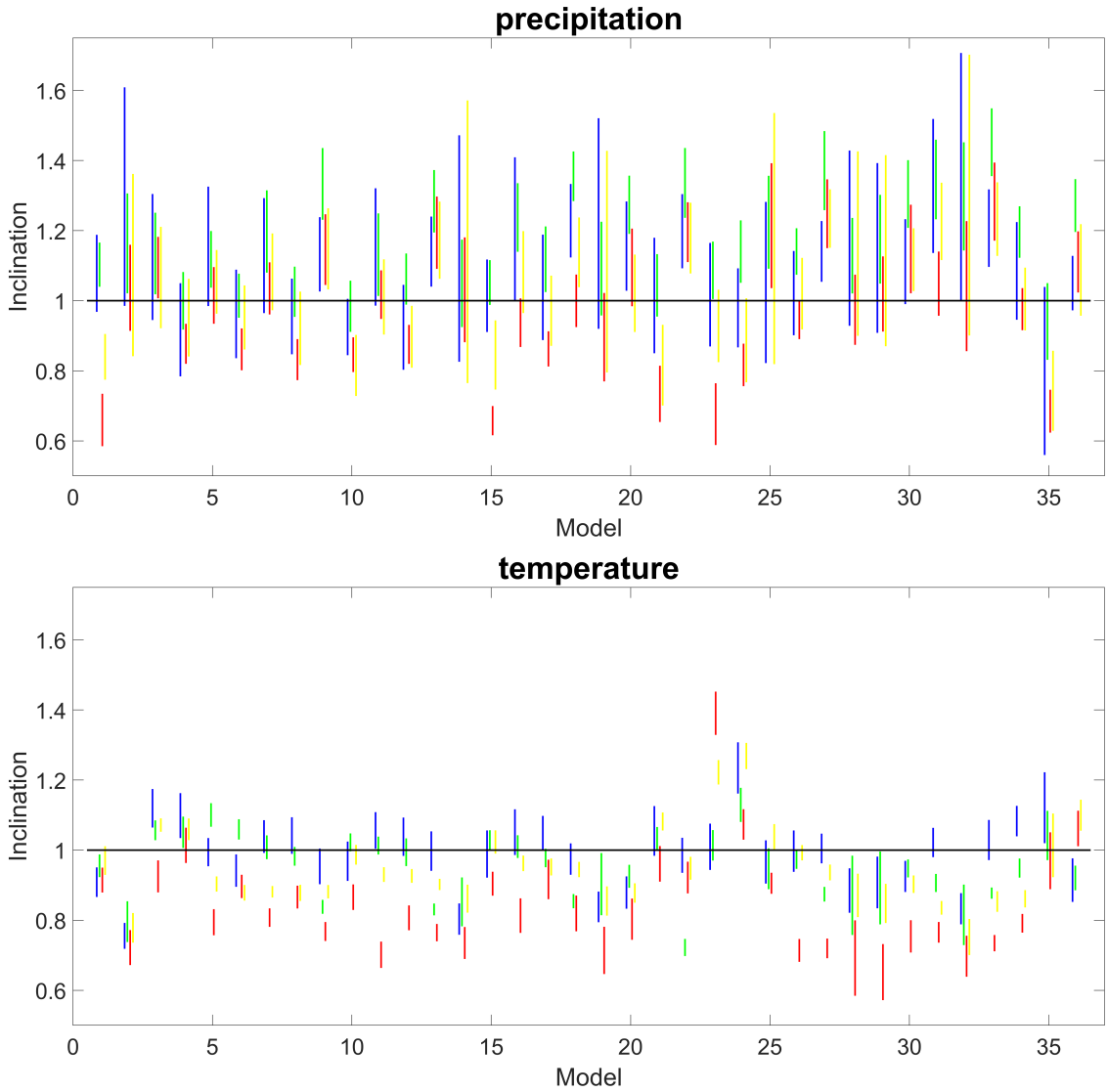

Figure 4: For RCP8.5 we show the inclinations of the robustly fitted lines used in the q-q mapping extensions, as explained in Figure 3. Top panel shows for precipitation while bottom panel shows for temperature. The coloured lines indicate seasons. Green is spring, red is summer, yellow is autumn, and blue is winter values. The length of the lines indicate spread over models.

Table 2: List of the 15 CORDEX model combinations used in the cross-validation experiments aiming on determining best method for time-series calibration. As Climate Atlas is continuously updated, these models are a subset of what is currently used in the atlas – see Table 7 for the current list.

	Global model	Regional model
0	MPI-M-MPI-ESM-LR	CLMcom-CCLM4-8-17_v1
1	MPI-M-MPI-ESM-LR	MPI-CSC-REMO2009_v1
2	MPI-M-MPI-ESM-LR	SMHI-RCA4_v1a
3	CNRM-CERFACS-CNRM-CM5	CLMcom-CCLM4-8-17_v1
4	CNRM-CERFACS-CNRM-CM5	SMHI-RCA4_v1
5	ICHEC-EC-EARTH	CLMcom-CCLM4-8-17_v1
6	ICHEC-EC-EARTH	SMHI-RCA4_v1
7	ICHEC-EC-EARTH	KNMI-RACMO22E_v1
8	ICHEC-EC-EARTH	DMI-HIRHAM5_v1
9	IPSL-IPSL-CM5A-MR	IPSL-INERIS-WRF331F_v1
10	IPSL-IPSL-CM5A-MR	SMHI-RCA4_v1
11	MOHC-HadGEM2-ES	CLMcom-CCLM4-8-17_v1
12	MOHC-HadGEM2-ES	DMI-HIRHAM5_v1
13	MOHC-HadGEM2-ES	KNMI-RACMO22E_v2
14	MOHC-HadGEM2-ES	SMHI-RCA4_v1

When comparing the calibrated models with the 'truth' we are interested in the distributional differences. These are here estimated with the mean, the standard deviation, and the Kolmogorov-Smirnov statistics. The latter measures the maximal distance between the two cumulative distributions and therefore provides an overall measure of the difference between the distributions.

We are interested in comparing simple mean adjustment and *q*-*q* transforms for both δ-change and bias correction.

3.3 Results

Figure 5 shows an example which demonstrates the difference between the δ-change and the bias correction. The top panel shows the time-series in the calibration period. Comparing the green and the blue curves we see that the model is too warm. From the bottom panel we see that this also holds in the future. In the bottom panel, the red curve is the bias corrected series, and the cyan is the δ-change calibrated series. We see that both the calibrated series fit the mean value of the 'truth' better than the uncorrected series. Note that we cannot be sure that this is always the case: the climate change in model and 'truth' could be different and conspire in a way to make the effect of the calibrations negative. Note, also as mentioned before that

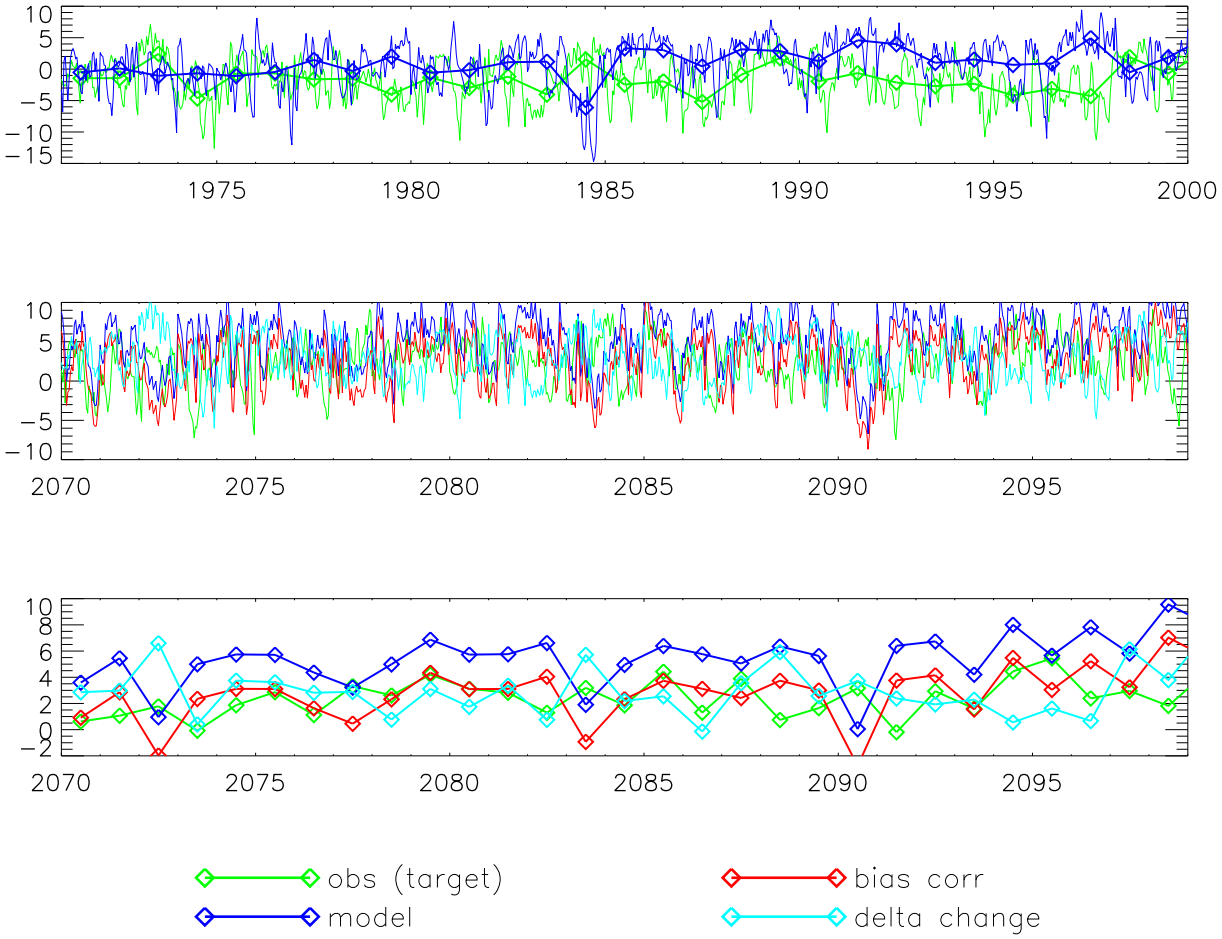

Figure 5: Time-series demonstrating simple mean bias correction. This is January near-surface temperature. Calibration period 1971-2000 (upper panel), prediction period: 2070-2099 (bottom panel). Scenario: RCP8.5. As observation is used model number 3, and for model number 14. Thick curves are monthly means, thin curves are daily values.

the δ-change calibrated series has the same temporal characteristics as the observations while the bias corrected series has the characteristics of the model.

We are now ready to describe the results of the cross-validation experiments. The next figures show results in a matrix form where the ordinate indicates the model chosen as 'truth' and the coordinate the model chosen as model. Figure 6 shows the difference of the mean climatology in the future between the calibrated models and the 'truth'. The top panel shows the difference without any calibration, i.e., just the difference between the model and the 'truth'. The second and third rows show the differences based on the calibrated values. In the second row the calibrations are done on monthly means, in the third row on daily values. Values close to zero are good. First, we note that any calibration is better than no calibration. Although not extremely obvious from these plots we find that in general bias correction is better than

Figure 6: The difference between mean climates in calibrated models and 'truth'. January near-surface temperature. Calibration period 1971-2000, prediction period: 2070-2099. Scenario: RCP8.5. The numbers on the axes refer to the model combinations in Table 2. The horizontal axes indicates the model selected as 'truth'. Top panel shows uncalibrated values. In middle panes calibration is performed on monthly means, in lower panels on daily means.

δ-change and that it is better to do the calibration on daily values than on monthly means. However, note that these conclusions hold for the average over many 'truth'/model combinations. There is a large scatter in the plots and for some combinations of 'truth'/model the calibrations have not improved the model.

Figures 7 and 8 show results for the difference between standard deviations and for the KS statistics. The KS-statistics is always positive and values close to zero indicate that the distribution of the two time-series are similar. The conclusions from the last paragraph based on the mean climates are confirmed.

Until now we have focused only on monthly means of the surface temperature in January in the late century. We summarise these results in plots like those in Figure 9. We also have results for precipitation, for other months, for other periods, and for daily means (not shown).

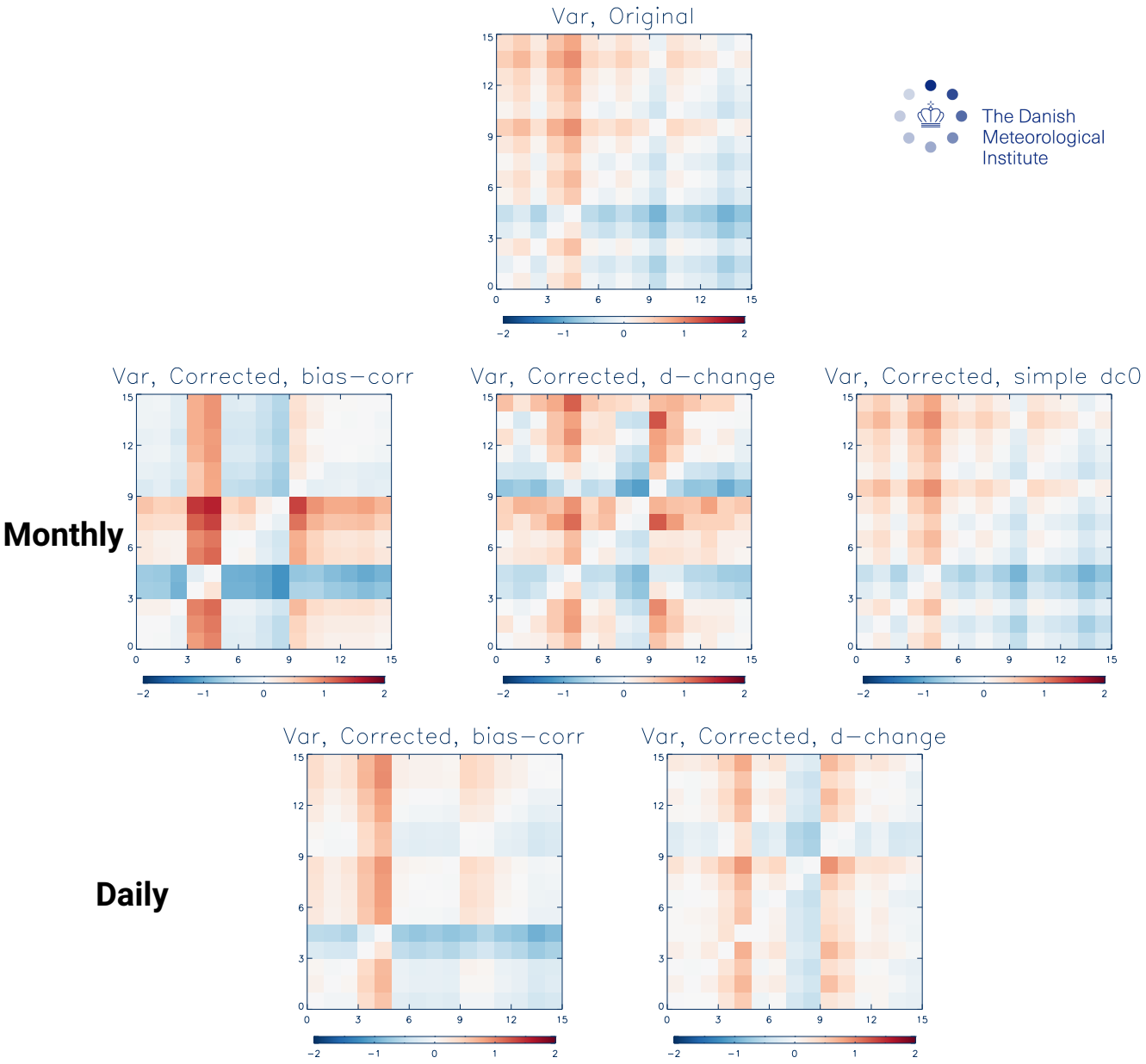

Figure 7: The difference between the variability (standard deviations) in calibrated models and 'truth'. January near-surface temperature. Calibration period: 1971-2000, prediction period: 2070-2099. Scenario: RCP8.5. The numbers on the axes refer to the model combinations in Table 2. The horizontal axes indicates the model selected as 'truth'. Top panel shows uncalibrated values. In middle panels calibration is performed on monthly means, in lower panels on daily means.

It is interesting to study the effect of the length of the calibration period. Figure 10 shows results for the settings as Figure 9 but for a shorter calibration period. We see that results have worsened and there is now only little difference compared to the situation without any calibration.

3.4 Conclusions

Based on the cross-validation experiments described above we draw the following conclusions:

- In general, bias correction seems to be the best method.

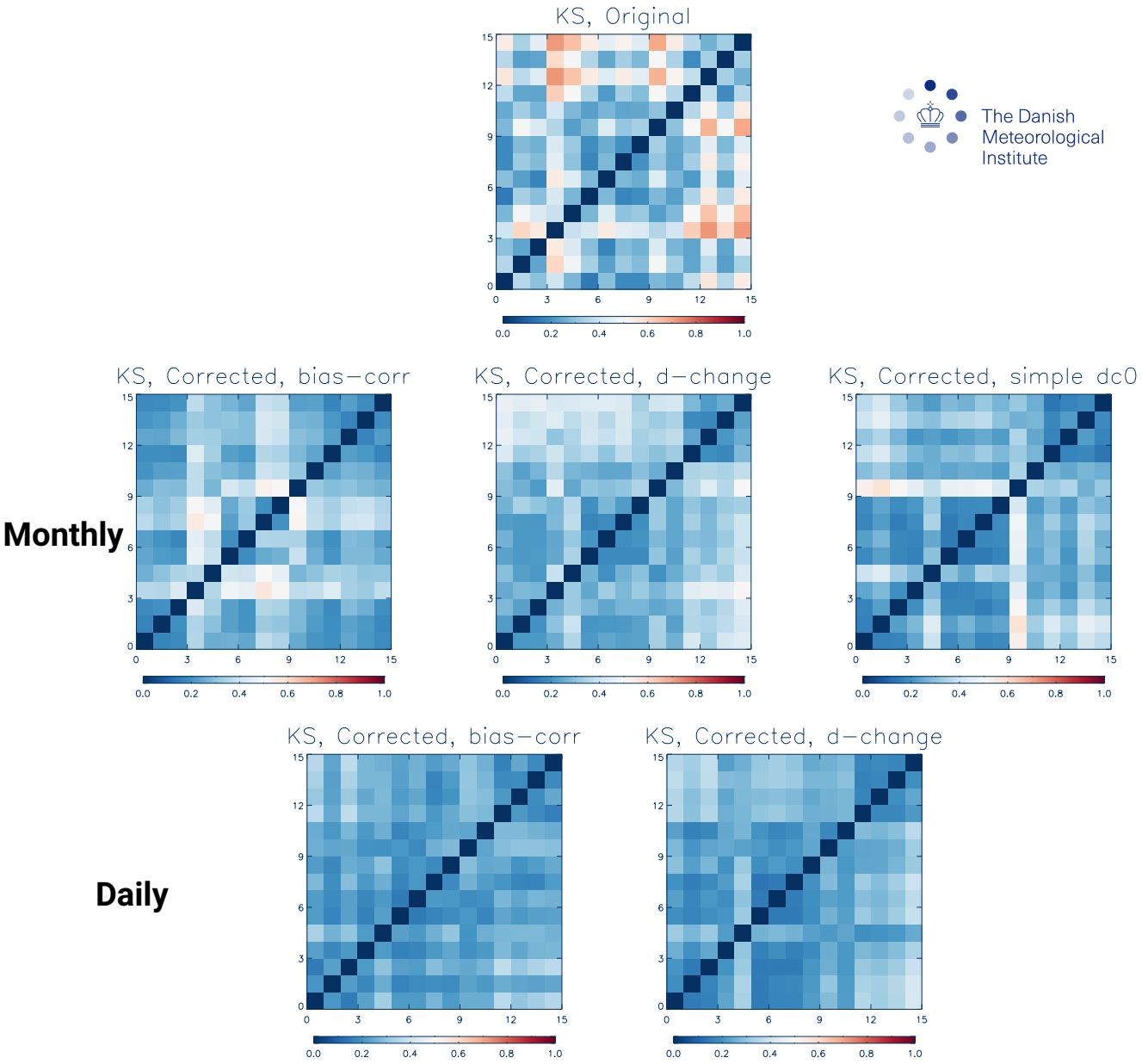

Figure 8: Kolmogorov-Smirnov statistics for January near-surface temperature. Calibration period 1971-2000, prediction period: 2070-2099. Scenario: RCP8.5. The numbers on the axes refer to the model combinations in Table 2. The horizontal axes indicates the model selected as 'truth'. Top panel shows uncalibrated values. In middle panes calibration is performed on monthly means, in lower panels on daily means.

- Bias correction should be performed on daily data even if only monthly means are wanted.

There are some other considerations:

- Results are sensitive to length of calibration period, but in the Danish Climate Atlas the impact is minor since 30-year periods of calibration data are available.
- Bias correction gives temporal correlations as in model, not as in observations.
- For δ-change, the length of the calibrated series is limited by the length of the observations.

We emphasise that these conclusions hold only for the average over many realizations and the situation may be different for a particular 'truth'/model combination. The conclusions are

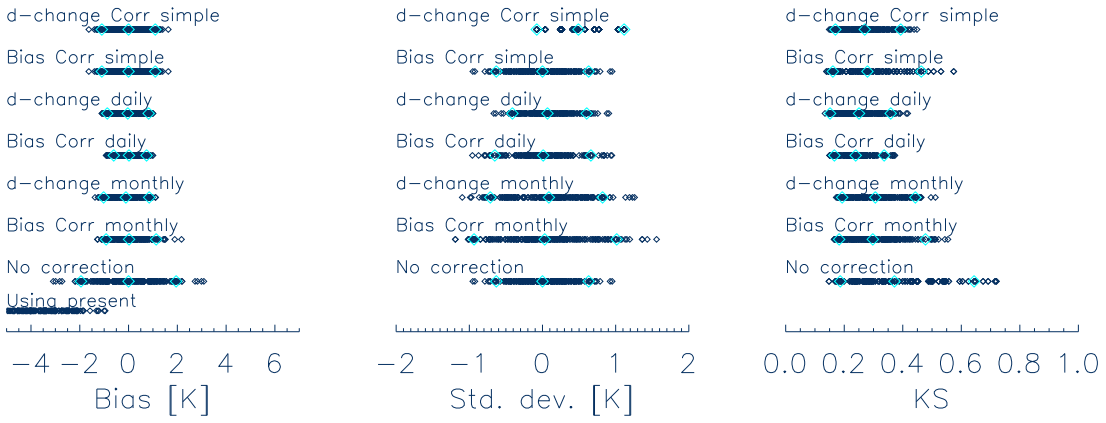

Figure 9: Summary of the cross-validation results for January near-surface temperature. Calibration period 1971-2000, prediction period: 2070-2099. Scenario: RCP8.5. The columns are: mean, standard deviation, and KS. For each method the 15*14 cross-validation results are shown by dots. Blue diamonds mark average, and upper and lower 5 percentiles.

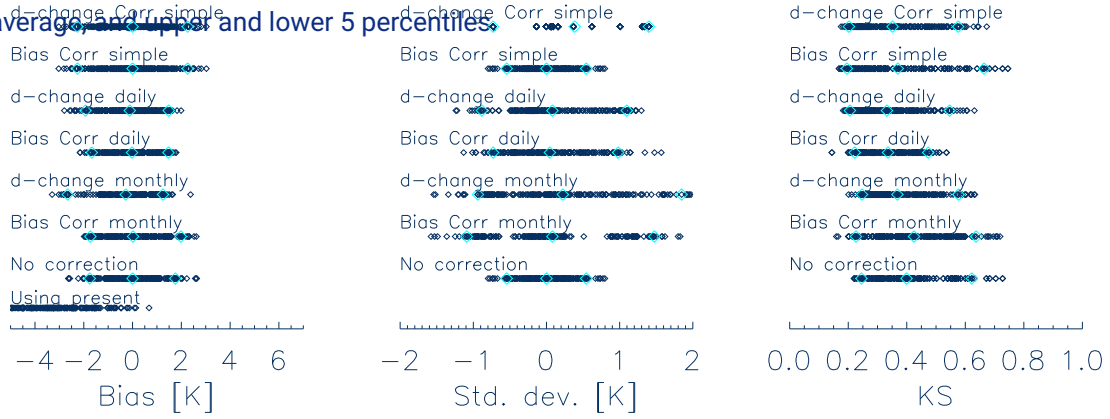

Figure 10: As Figure 9 but for a shorter calibration period, 1985-2000.

probably somewhat on the optimistic side as they are based on model/model comparison and not on real observations.

4 Calibration of extreme precipitation

4.1 Short introduction

Extreme events occur rarely by nature and therefore the empirical quantile-quantile calibration technique applied in Section 3 cannot be used, since the tail of the empirical cumulative distribution function (CDF) is poorly defined. Therefore, for extreme events, extreme value analysis is applied, where the empirical CDF is replaced by an analytically formulated cumulative distribution function, as described below.

4.2 Extreme value analysis

In extreme value analysis (EVA) one considers a time series of e.g. hourly values, and the aim is to estimate the frequency of occurrence of rare events, often expressed as the T-year return level, which is the level that on average is exceeded once every T years. Two main methodologies have been developed within EVA: the classical and the peak-over-threshold (POT) method. For reference and more details, see Coles [2001].

In the classical method, one considers the statistical distribution of the maximum value over a time-'block', often a year. It can be shown, that under very general conditions, the CDF of the series of block maxima converges to the generalised extreme value (GEV) distribution given by

$$F_{GEV}(x) = exp\left[-(1-\xi\frac{x-\mu}{\sigma})^{1/\xi}\right] \tag{1}$$

The GEV distribution has three parameters. The location μ describes the location of the distribution and the scale parameter σ describes the width of the distribution. The ξ is the shape parameter and describes the character of the upper tail of the GEV-distribution. $\xi > 0$ implies a thin tail, while $\xi < 0$ implies a heavy tail, which usually is the case for extreme precipitation events[1]. The T-year return level, i.e. the level that is, on average, exceeded once every T years is given by

$$x_T = F^{-1}_{GEV}(1-\frac{1}{T}) \tag{2}$$

In the peak-over-threshold (POT) method, all peak values above a specified threshold x_0 and separated by a minimum time span are considered. It is assumed that peak occurrences are independent and Poisson-distributed with parameter λ, which is the average number of exceedances (events) per year. Alternatively, λ can be specified, in which case x_0 is a stochastic variable.

[1] Be aware that two different sign conventions for ξ are used in the literature

It can be shown that under very general conditions the distribution of the peak exceedances $x - x_0 > 0$ are distributed as a Generalised Pareto distribution (GPD) with cumulative distribution function given by

$$F_{GPD}(x - x_0) = 1 - \left(1 - \xi \frac{x - x_0}{\sigma}\right)^{1/\xi}, x > x_0. \tag{3}$$

The T-year return level is determined as the level exceeded on average once every T years, and therefore the following holds:

$$\lambda T[1 - F_{GPD}(x_T - x_0)] = 1 \tag{4}$$

from which we get

$$x_T = F^{-1}_{GPD}(1 - \frac{1}{\lambda T}) + x_0. \tag{5}$$

Both for the classical and POT methods, σ is the increase in x_T when T changes from 1 to 10, while ξ defines x_T when $T \to \infty$.

There are several procedures available for estimating the parameters from data, the most important being: maximum likelihood (ML), method of moments (MOM) and probability-weighted moments (PWM). Hosking and Wallis [1987] and Hosking et al. [1985] demonstrate that PWM in general yields reliable results with low variance for the number of samples in this study, whereas in particular ML can be problematic. Therefore we use PWM in the following.

4.3 Applications of calibration methodologies based on EVA

In Section 4.2 the theoretical framework was presented for estimating extreme value distributions and associated return levels. This leads to a number of ways to obtain future projected values and climate factors, defined as the ratio between a future and a present value, which will be presented below.

4.3.1 Scaling factor on the return levels

The simplest calibration approach is to assume a climate factor on the return level, e.g. Larsen et al. [2009]

$$\tilde{M}_{f,T} = \underbrace{\frac{M_{f,T}}{M_{c,T}}}_{\delta\text{-change factor}} \times O_T = \underbrace{\frac{O_T}{M_{c,T}}}_{\text{Bias correction factor}} \times M_{f,T}, \tag{6}$$

We note that in this case the δ-change and bias correction methods are identical.

4.3.2 Scaling factor on the parameters in the POT model

We assume scaling factors on the parameters in the POT-model, e.g., defining the calibration transformation, as in Arnbjerg-Nielsen [2012]. Thus, if k is an arbitrary POT-parameter, we have:

$$\tilde{k}_{M_f} = \underbrace{\frac{k_{M_f}}{k_{M_c}}}_{\delta\text{-change factor}} \times k_O = \underbrace{\frac{k_O}{k_{M_c}}}_{\text{Bias correction factor}} \times k_{M_f}, \tag{7}$$

4.3.3 Analytical quantile matching

Kallache et al. [2011] and Laflamme et al. [2016] apply a transformation methodology for extreme values, based on analytical quantile-matching applicable for both the classical and the POT methods.

In the bias correction approach, we make use of Equation 5 above, which is valid both for M_c and for O and for any return period T. If we apply this to O and M_c we obtain the expression

$$(1 =)\lambda_{M_c} T[1 - F_{GPD,M_c}(M_{c,T} - M_{c_0})] = \lambda_O T[1 - F_{GPD,O}(O_T - O_0)] \tag{8}$$

relating $M_{c,T}$ and O_T, and after some manipulation, we arrive at

$$O_T = F^{-1}_{GPD,O}\left\{1 - \frac{\lambda_{M_c}}{\lambda_O}\left[1 - F_{GPD,M_c}(M_{c,T} - M_{c_0})\right]\right\} + O_0 \tag{9}$$

Thus, Equation 9 defines a transformation from $M_{c,T}$ to O_T, which then in the calibration procedure is applied to $M_{f,T}$ to obtain $\tilde{M}_{f,T}$. As discussed in section 4.6, this is the method chosen.

In the δ-change approach, a transformation corresponding to the one above can be formulated.

4.3.4 Spatial aggregation

The procedure of EVA and its subsequent application to calibration and projection is done on every grid point and therefore projected future return levels are given as a spatial field. These, however, often contain regional variations which are artificial in the sense that they are due to too short series to base the EVA on.

To overcome this, an alternative approach is to combine data from neighbouring grid points to get aggregated results valid over a wider region [Buishand, 1991]. One approach is to do the EVA on a grid point basis and then *area-average* the parameters obtained by the EVA, to get results representative for the region. Alternatively, there is the *station-year* method, where series from neighbouring grid points are combined into one long series, on which the EVA is performed. This requires that the series are independent and therefore a minimum separation distance is required. We choose a minimum distance of 30 km in agreement with Buishand [1984].

4.4 Realism of the models used

To check the realism of the models used, we calculated return levels of all models based on the area-averaged aggregation, which are compared with similar return values based on observations (see 4.6.1). Results are shown in Figure 11.

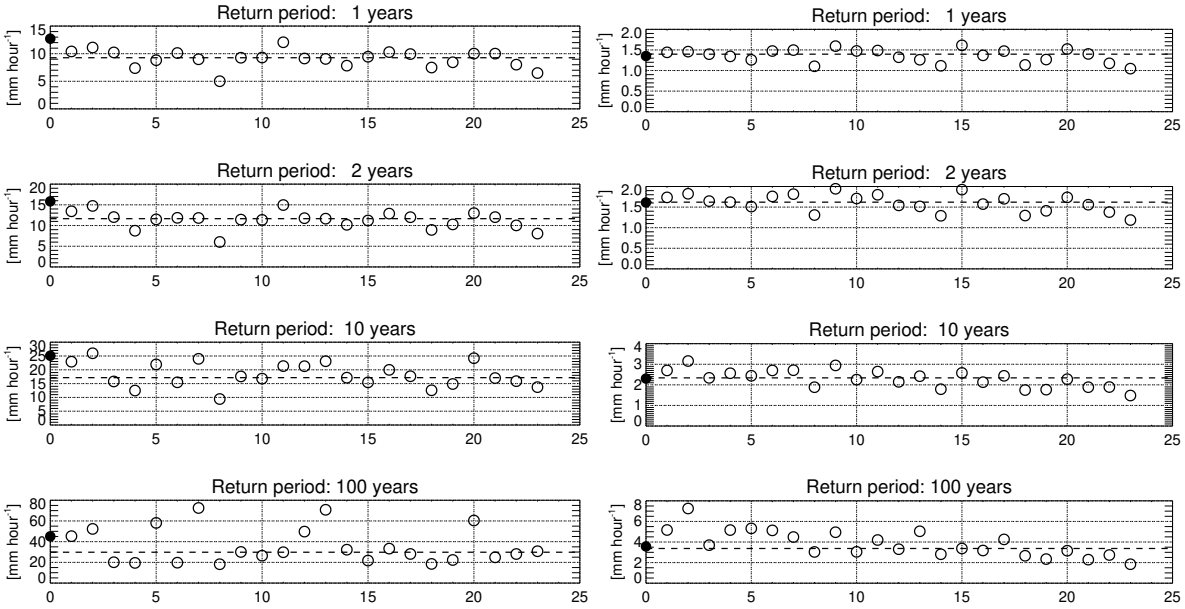

Figure 11: Return values from observations (NRM, filled circles) and from raw (not calibrated) model data in the calibration period (open circles) for 1, 2, 10, and 100 year return periods and for 1 hour (left panel) and 24 hour (right panel) duration. In each sub-panel, the different models are displayed along the x-axis, and the dashed line is the model median.

These plots show that there is already an acceptable agreement between the return levels from observations and the ones based on raw, not yet calibrated model data. Calibration is therefore likely to add skill and does not have to deal with large initial offsets between model and observations.

4.5 Inter-model cross validation

We performed inter-model cross-validation, as described in Section 3.2, to evaluate overall performance of the calibration methods and to see, whether a particular method or class of methods stands out as performing particularly well. We have 23 models available[2] and therefore can make $23 \times (23 - 1) = 506$ comparisons and display the statistical properties of the absolute error of the different calibration methods. We will evaluate the methods listed in Table 3.

From Figure 12 it is seen that for both the classical and POT methods, the *obs* and *sce* methods (incl. *obs-aa* etc.) have larger absolute errors than the calibration methods. This

[2] 23 models with hourly output were available in version v2019a. The extreme precipitation in Climate Atlas is currently based on 35 models (for RCP8.5). See the full list in Table 8.

Table 3: Overview of methods and sub-methods for obtaining future return levels. See Section 4.3.

obs	Present–day observed
sce	Local scenario from RCM
retfac	Scaling of return levels
parfac	Scaling of EVA parameters
dc	δ-change of local return value with local parameters
bc	Bias correction of local return value with local parameters
dc-s/bc-s	δ-change/bias correction of local return value with local location and scale parameters and area-averaged shape parameter
dc-sr/bc-sr	δ-change/bias correction of local return value with local location and scale parameters and area-averaged and 'reduced' shape parameter
dc-ss/bc-ss	δ-change/bias correction of local return value with local location parameter and area-averaged scale and shape parameter
dc-lss/bc-lss	δ-change/bias correction of local return value with area-averaged location, scale and shape parameter
obs-aa	As obs, but on area-averaged data
obs-sy	As obs, but on station-year data
sce-aa	As sce, but on area-averaged data
sce-sy	As sce, but on station-year data
retfac-aa	As retfac, but on area-averaged data
retfac-sy	As retfac, but on station-year data
dc-aa	As dc, but on area-averaged data
dc-sy	As dc, but on station-year data
bc-aa	As bc, but on area-averaged data
bc-sy	As bc, but on station-year data

shows that applying a calibration method potentially decreases the error. We also note that the error of the adjustment methods exhibit no big difference between the classical and the POT methods. Then there are the adjustment methods: *retfac, parfac, dc* and *bc* including their aggregated variants. Here there are no big differences among methods in terms of absolute error, but the *bc* methods show the smallest absolute errors.

Similar plots for 24 h average precipitation are shown in Figure 13. Here, errors are in general smaller for the POT methods compared to the classical methods. The *obs* methods have the largest absolute errors, but the *sce* methods seems to perform comparably to the adjustment methods.

4.6 Practical implementation

The Climate Atlas provides return levels for 2, 10 and 100 year return levels, and for 1 h- and 24 h-summed precipitation values[3]. Since we want to use the same approach for 1 h- and 24 h-

[3]Since this initial analysis, Climate Atlas has been expanded and now provides 2, 5, 10, 20, 50 and 100 year return levels for 1 and 24-hour precipitation.

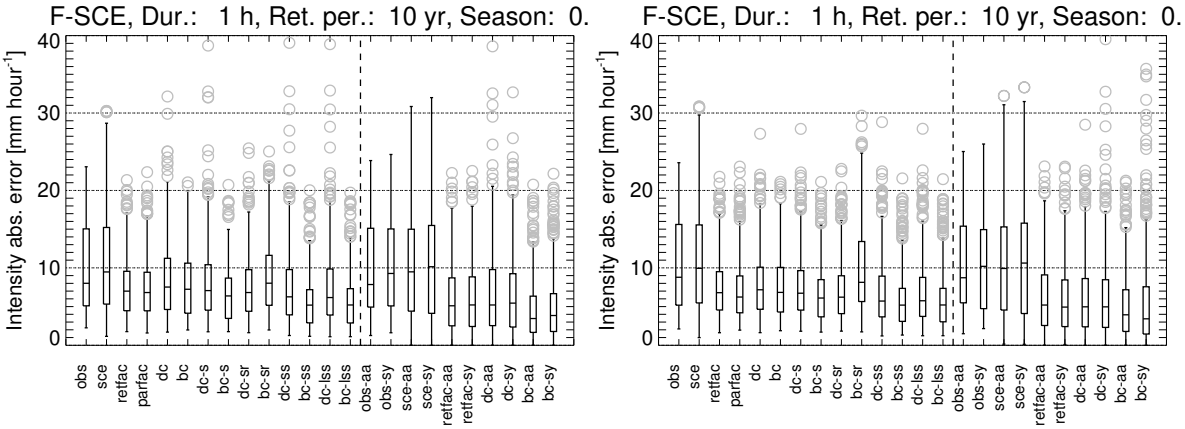

Figure 12: Box-Whisker plot of absolute error calculated over the Danish region between 'future-observed' and projected 10-year return value of 1 hour average precipitation for 2070-2100 scenario period from RCP8.5 runs using the classical method with one year block length (left) and the POT method with 3 events/year (right). For abbreviations of adjustment methods, see Table 3. Methods to the right of the dashed line are *aa*- and *sy*-aggregated methods. The boxes enclose the .25/.75- range. The whiskers extend out to the minimum/maximum of the data, or to 1.5 times the .25/.75- range, if there is data beyond these. Outliers are marked with circles.

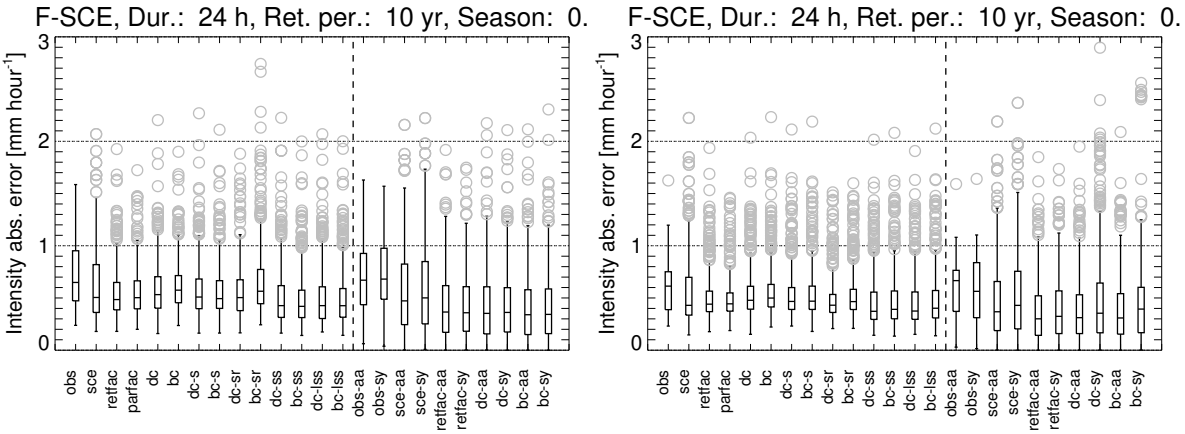

Figure 13: As Figure 12, but for 24 h precipitation.

precipitation, we decided to use the *bc* method, corresponding to Equation 9 (with geographical variations included).

4.6.1 POT-parameters from observations

We follow closely the method described in [Gregersen et al., 2014b,a, Madsen et al., 2017]. In this method, the local, geographically varying parameters in the POT for several durations (of which we make use of the one and 24 hours), are given as linear functions of explanatory variables, derived from gridded daily precipitation totals from Klimagrid Danmark over the period 1989-2010 see (section 2.1) using regression. The explanatory variables are: 1) the mean

annual precipitation and 2) the mean daily exceedances over a threshold of z_0 = 19.2 mm/day. Using mean exceedances is an alternative formulation of the GPD distribution. The regression coefficients linking the Poisson parameter, and mean exceedances (equivalent to the scale) are given in Gregersen et al. [2014b], while the shape parameter has been given by Gregersen (pers. comm.)

4.6.2 POT parameters from models

EVA was done on precipitation data from a number of different GCM-RCM combinations – see Table 8. These have in general different precipitation characteristics. Therefore, we use a different censoring than for the observations, in that we specify λ = 3 events/year and determine a z_0, varying spatially and between models. Peaks in the rain intensity should be separated by 24 hours or more to count as separate events.

4.7 The final procedure

Based on the considerations above, we apply the *bc* method with spatial variations. Thus, according to Equation 9 a transformation is established between the present-day model and the observations based on the analytical quantile mapping, and subsequently this transformation is applied to return levels from the scenario to give as output calibrated future return levels.

4.8 Cloudbursts

The definition of a cloudburst is, as stated before, precipitation exceeding 15 mm in 30 minutes, but none of the CORDEX models have this temporal resolution represented in their output. Therefore an alternative approach has been chosen. In the DMI Technical Report 19-06 [Cappelen, 2019], station observations in high temporal resolution have been analysed for the period 2011-2018. In an average year, 87 stations out of 258 have measured at least one cloudburst. This roughly corresponds to one every 3 years for the given network of stations, ignoring any regional variation in the probability. The 'calibration period' for cloudbursts is therefore 2011-2018.

With the assumption that the occurrence of cloudbursts is associated with extremes in hourly precipitation, which is readily available from models, we use hourly precipitation with a present-day return period of 3 years as a proxy for the occurrence of cloudbursts.

The change in 3-year return-level in hourly precipitation can be obtained from the parameters of POT fits to present-day and future extreme precipitation. From the present-day parameters, the three-year return level can be obtained for each point. This value is now entered into the corresponding CDF for the future period, and the return frequency of this value can be calculated. The uncertainty is calculated as the pointwise spread among models.

5 Mean sea level rise

5.1 Introduction

Information on climate change is assessed by IPCC. In 2013, IPCC released their 5th assessment report (AR5), giving best estimates and likely ranges of sea level change on global and regional scale [Church et al., 2013b]. In 2019, IPCC released a Special Report on the Ocean and Cryosphere in a Changing Climate (SROCC) [Oppenheimer et al., 2019]. In SROCC, two important aspects of sea level are noted initially for understanding the climate change induced sea level rise (SLR): climate change induced global mean sea level (GMSL) rise (introduced in this section) and extreme sea level (ESL) rise (Section 6).

5.1.1 Global mean sea level rise

There are clear links between rising temperature and GMSL rise. Observed and projected GMSL rise has two major components; thermal expansion (increase in the volume of ocean water caused by additional heat uptake) and melt water input to the ocean from retreating land-ice (glaciers and ice sheets). Other contributions include for example changes in land water storage. The thermal expansion effect is included in coupled ocean-atmosphere climate models. The melt water input from ice sheets is presently not included in the global climate models assessed in SROCC and AR5, but is added to the GMSL signal afterwards [Slangen et al., 2017]. In SROCC, it is clear that Antarctica is a source of major uncertainty in the estimation of future SLR, and will have a positive net contribution on GMSL rise.

To get a better understanding of the melt water input from ice sheets, intense research is ongoing internationally, and it is expected that more precise knowledge will become available in the coming years. At present, it is internationally acknowledged that there is a small but not negligible risk of large and rapid changes especially from Antarctica, which would lead to rapid sea level rise (e.g. [DeConto and Pollard, 2016, Bamber et al., 2019]), and that sea level rise will continue for centuries, with a speed that heavily depends on greenhouse gas emissions [Oppenheimer et al., 2019].

5.1.2 Local sea level rise around Denmark

Sea level change is not evenly distributed around the globe. Differences occur mainly due to gravitational and elastic effects in relation to melting ice (regional scales), effects of regional ocean dynamics (changes in current systems) and regional steric effects (that is, ocean volume changes due to regional changes in temperature and salinity).

Changes in the Earth's gravity field and elastic deformation of the solid Earth give rise to spatial differences in the sea level rise pattern [Mitrovica and Milne, 2003]. For example, near an ice sheet losing mass in the Antarctic, reduced gravitational attraction between the ice and

the nearby ocean causes sea level to fall, despite the global sea level rise [Mitrovica et al., 2011]. In the Climate Atlas, we adopted the factor of 1.1 for the sea level signal from Antarctica for the whole of Denmark, following the sea level fingerprint from Mitrovica et al. [2009].

Regional ocean dynamics, that is, ocean currents, have an associated sea level signal. For instance the Gulf Stream has a sea level signal of about 1 m. A change of ocean currents will have an impact on sea level change. Similarly, a change in the average wind patterns in coastal areas changes the push of the wind on the water towards the coast, giving rise to local sea level change. The dynamic effects are included in ocean models of climate change depending on scales resolved.

Regional steric effects occur if the salinity of the regional ocean changes, or the change in temperature is different from the global mean. The effects are included in ocean climate models.

The local coastal sea level ($\sim$ 10km) is affected by global, regional ($\sim$ 100km) and coastal features (e.g. regional land rise and local subsidence).

Regional/local land rise in Denmark has been assessed by DTU Space. Overall, all of Denmark is rising due to glacial isostatic land rise in Scandinavia after the last ice age. The land rise of northern Denmark is about 2 mm per year, decreasing towards south and west, to zero just south of the Danish border (Personal communication, Per Knudsen, DTU Space, 2016). In the past, this has compensated for external sea level rise, giving an average relative sea level decrease in the northern-most part of the country in the 20th century [Hansen, 2018].

5.1.3 Observed mean sea level and change

Globally, GMSL of the last centuries is well documented, including acceleration after the 19th century [Church et al., 2013a, Bamber et al., 2018]. Over the last two centuries, estimated GMSL rise mostly relies on coastal tide-gauge measurements. The average estimate is 1.4 mm yr^{-1} for the period 1901-1990 based on two recent reconstructions by Hay et al. [2015] and Dangendorf et al. [2017]. High precision satellite altimetry started in October 1992, providing altimetry-based ocean wide estimates of GMSL rise. Average GMSL increased to 3.2 mm yr^{-1} over the period 1993-2015 [Watson et al., 2015, Nerem et al., 2018], reflecting an acceleration in recent decades.

In Denmark, the local sea level has been measured with tide gauges since the end of the 19th century. Monthly and annual mean sea level from the 14 stations with more than 20 years of data is published in Hansen [2018] and reported to PSMSL [Holgate et al., 2013]. Sea Level is measured relative to a local datum, which can be directly converted to the Danish national height system DVR90. This was designed to approximately match the mean sea level around Denmark in 1990. The mean sea level of the Climate Atlas reference period (1981-2010) for the 14 stations in Hansen [2018], relative to DVR90, is listed in Table 4. However, these numbers should be used with some care, as many data are missing, especially from the 1980'es. This introduces a high bias, as the sea level has generally been rising throughout the period.

Table 4: Relative mean sea level (cm) at 14 Danish stations 1981-2010, height system DVR90, derived from Hansen [2018]. Years with more than 10% missing data have been left out in the calculation.

Station	Sea level [cm]	Station	Sea level [cm]
Hirtshals	-7	Slipshavn	3
Frederikshavn	-5	Korsør	5
Hanstholm	-1	Hornbæk	4
Århus	2	København	8
Fredericia	1	Rødbyhavn	6
Esbjerg	7	Gedser	7
Fynshav	1	Tejn	2

5.2 Methods

5.2.1 Dedicated modelling effort

We performed the HBM climate simulations for five periods, i.e. historical period, 1981-2010; RCP 4.5 period, 2041-2070; RCP 4.5 period, 2071-2100; RCP 8.5 period, 2041-2070; RCP 8.5 period, 2071-2100. For detailed description of HBM please refer to Section 8.2.2.

Ensemble simulations using EURO-CORDEX members are ongoing throughout the Climate Atlas project. Before the Climate Atlas release 2019, we were able to perform two simulations using the meteorological forcing from two CORDEX members: DMI-HIRHAM5_v1 (Nr. 8 and in Table 2) and SMHI-RCA4 (Nr. 6 and in Table 2). In version v2020b, we have added one additional experiment based on CORDEX member DMI-HIRHAM5_v2.

5.2.2 Localising global mean sea level rise

A general introduction to local sea level rise around Denmark is given in Section 5.1.2. Here we present how to obtain the local sea level rise values. The localising methodology follows the previous work described in Olesen et al. [2014], and the main procedure is as listed below.

1) Obtain the electronic data from supplement materials in Church et al. [2013b] and the new input of GMSL rise from Oppenheimer et al. [2019] (described in Section 5.1.1). The data from IPCC includes the median value (50%) and the likely range (upper 83% and lower 17% limits).

2) In the first step of the data processing, glacial isostatic adjustment (GIA) is deducted, since more detailed regional land rise is used in Climate Atlas (Section 5.1.2).

3) It is evident that sea level change varies from the North Sea Danish coast to the Baltic Danish coast, the primary cause is different treatments of inner Danish water coastlines in the global climate models. To obtain the sea level change for the whole Denmark without artificial coastal effects, we averaged the values from two points; one point in the North Sea (54.5 °N, 4.5 °E) and one point in the southern Baltic Sea (56.6 °N, 18.5 °).

4) Scale to the Climate Atlas reference period. In Climate Atlas, we used reference period 1981 - 2010 and 30 year time slices. However, all the IPCC SLR projections used the reference period 1986 - 2005 and 20 year time slices. Therefore, projected SLR is scaled to the Climate Atlas reference period according to a quadratic formula.

5) The importance of mean sea level change caused by local ocean dynamics and steric effects has been evaluated by averaging 30 years sea level data from HBM simulations for each period. We found this contribution at the end of the century varies between -1.5 cm and -0.4 cm . We, therefore, considered this change within the uncertainty range, and thus too small to be significant. It has been left out of the further calculations.

6) The likely range of the IPCC provides lower and upper limits (17% and 83%). 10 and 90 percentiles are calculated from the likely range of IPCC, based on a symmetric normal distribution. For the 10-percentile, this is considered a good approximation. For the 90 percentile, the method should give a lower limit estimation of the true uncertainty, especially for the RCP8.5 scenario, but the method is chosen because it is simple and well-described.

7) All values were corrected for regional land rise, to provide the relative sea level signal, according to section 5.2.5.

5.2.3 The 95-percentile

There is a small but significant risk of rapid sea level rise outside the likely estimates, which is mirrored in relatively high numbers for the upper percentiles for global-sea level.

The present consensus on particularly the higher percentiles (95% and above) is that they cannot be constructed meaningfully by statistical analysis of data from the existing climate model ensembles, nor can they be constrained by dedicated model efforts. This is in part due to the lack of interactive glacier and ice sheet modules in the applied climate models and partly due to a limited physical understanding of the processes that have been suggested to lead to instabilities in the Antarctic Ice sheet as ocean and atmospheric temperatures increase. The latter includes two independent steps whereby the established impact of global warming is a loss of the floating ice shelves which in the following phase leave tall ice cliffs exposed that will collapse under their own weight; a process termed marine ice-cliff instability. This idea was first proposed by DeConto and Pollard [2016] and have been integrated into a very recent expert assessment addressing the high end percentiles [Bamber et al., 2019].

This expert judgement concludes that for a five degree warming there is a 5% risk that global mean sea-level will exceed 2.4m year 2100, where 1.8m is directly linked to ice sheet melting. This study appears to be contradicted by the more recent high impact paper by Edwards et al. [2019] that demonstrates that the proposed critical instability is far from certain and have likely not been in play during warm climates of the past. A full review on the topic is not the intention here, but in deciding on the recommendations here, consultations with Danish experts have been important. It is with this background the expert elicitation of Bamber et al. [2019] is chosen as the basis for a 95% percentile estimate. It is further the judgement that the experts contributing to the assessment were indeed informed about the forthcoming results

by Edwards et al. [2019] and that this knowledge has been incorporated into their judgement. It should also be noticed that 10% and 90% percentiles from Bamber et al. [2019] are largely consistent with SROCC's likely ranges.

To translate the value of 2.4 m to a 95% percentile for the RCP8.5 scenario and adjusting to the reference periods used in the Climate Atlas would imply several corrections of a few decimetres that will partly cancel out: a correction for temperature (negative), a correction to a centred reference period (negative) and a correction to Danish waters accounting for a large Antarctic contribution (positive). For transparency it is chosen not to do these steps and it is recommended to use 2.4 m directly as the best estimate available for the 95% percentile for RCP8.5 2071-2100. As global sea level rise is both one of the most certain (the sea level will rise) and uncertain (with regards to the range of the sea level rise) components of climate change and subject to intense investigations it can be expected that these numbers will be updated in future versions of the Climate Atlas.

5.2.4 Next centuries

Beyond 2100, global sea level rise will continue to increase with high confidence primarily due to continued thermal expansion and loss of ice from both Greenland and Antarctic ice sheets including contributions from both surface melting and dynamical mass loss. Two critical issues need to be observed when looking beyond year 2100. First, for Antarctica, the dynamical ice loss may include new instabilities such as the so called Marine-Ice-Cliff-Instability [DeConto and Pollard, 2016], but our physical understanding is limited and confidence low for this contribution, as also reported in new studies [Edwards et al., 2019]. For continued high global mean temperatures in the range of 1-4^{o}C, consistent with unchecked emissions (RCP8.5 and its Extended Concentration Pathways beyond 2100), the Greenland Ice sheet surface mass loss will be increasingly negative and a complete mass loss projected as a direct result over the next millennium or more. The exact path depends strongly on the emission scenario and there is medium confidence in the interval for the critical temperatures for irreversible and continued melt. Since AR5 new knowledge of the Antarctic contribution in particular explains why SROCC estimates are significantly higher. For RCP8.5 year 2300 the likely range of global mean sea-level rise is 2.3-5.4 m. With a large Antarctic contribution, numbers corrected to the Danish Waters will be slightly higher. Considering the large uncertainty this has not been pursued and no attempt is made to describe the regional differences due to land rise, which would generally be a negative local correction. DMI recommend to use the global estimates directly for Denmark, and to be prepared for updates of these multi-century numbers in the next years, as new knowledge appears.

5.2.5 Absolute and relative sea level rise

Absolute sea level describes the sea level in an "absolute reference frame", that is, a reference frame referring to the mass centre of the Earth. It is the quantity measured by satellite

altimetry and calculated in climate models. Relative sea level describes the sea level relative to the coast or a reference system fixed on land, and thus includes the effects of land rise and subsidence. In the online Climate Atlas, relative sea level changes are available for all coastal stretches, including the regional land rise signal from DTU Space (see section 5.1.2). For local applications, it may be relevant to further correct for local subsidence or rise effects.

5.3 Results

Since the national Danish height system DVR90 is designed to give almost-zero mean sea level in year 1990, just a few years before the centre of our reference period, and the measured sea level may have a bias towards high sea level (Section 5.1.3), we used 0 cm, relative to DVR90, as mean sea level for the reference period. This introduces an error of maximum 8 centimetres, when analysing the 14 tide gauge records in Hansen [2018].

With the method described above, the absolute sea level change is assumed to be the same for all coastal stretches in Denmark exposed to the open sea (Table 5). The median value for mean sea level rise is higher in the RCP8.5 scenario than in the RCP4.5 scenario, especially towards the end of the century, but with an overlap of the uncertainty intervals.

Table 5: Absolute mean sea level for Denmark [cm]. The values with brackets denote best estimate and 10 to 90 percentile ranges, while the values for 2300 give the likely range.

	Present day 1981-2010	Mid century 2041-2070	End century 2071-2100	2300 likely range
RCP4.5	0	26 [7-45]	42 [10-74]	230 - 540
RCP8.5		32 [8-57]	63 [19-108] 95-percentile 240	

Relative sea level rise varies from one coastal stretch to the next. The relative sea level rise for individual coastal stretches can be viewed in the online Climate Atlas. Overall, the relative sea level changes are positive in all regions (the sea level is rising), with higher values towards south and west, where the compensation from land rise is smaller. Except for this, the pattern is the same as for the absolute sea level.

6 Future extreme sea level events

6.1 Introduction

Changes in tides, storm surges, waves and other processes (e.g., coastal erosion, change of coastal ecosystems, salinisation of soils, saltwater intrusion into ground and surface waters etc.) are superimposed on the slowly increasing mean sea level. Changes in, and interactions between, each of these processes can cause water level variability to become of an even higher concern in the future. Understanding the combined future impact of these physical processes is a big challenge. This is especially true for the local scales considered in the Climate Atlas. The finer scale requires detailed knowledge of bathymetry, with high resolution, erosion processes and sedimentation, as well as wind fields with very high resolution in both time and space. Furthermore, the potentially increasing risk of compounding effects, such as storm surges and SLR, need to be assessed. Therefore, a detailed hydrodynamical model has been developed and operated at DMI for operational storm surge modelling [Berg and Poulsen, 2012]. This model serves to provide sufficient details and knowledge for Climate Atlas, where the model is run with atmospheric forcing from climate models and using the same high level of detail in coastline and bathymetry as in the operational model setup.

Extreme sea levels (ESLs) typically occur in association with storms [Pugh, 1987]. Such temporary raising of the water level originate from a combination of the wind stress acting on the sea surface and lowered air pressure (inverse barometer effect). Depending on the wind direction, the wind stress may generate ocean currents directed towards the shore. In shallow regions where the smaller water depth prevents a deeper return flow of water, the net shoreward transport can cause water to pile up along the coast, resulting in extreme water levels. The total still water level during the passage of storms also depends on the mean sea level and, in tidal regions, the timing of the tidal cycle. In the Western Baltic further contributions to the water level can arise from pre-filling of the Baltic Sea and from standing waves (seiches) in the basins [Samuelsson and Stigebrandt, 1996].

In Denmark, water levels which exceed the 20-year return level (Section 4.2) are defined as storm surges by the Danish Storm Council. There is a large variation of local 20-year return levels, due to e.g. variable tidal range and wind conditions between different locations.

6.1.1 Storm surges today and usage for coastal planning – with caution

The present day storm surge statistics used for the reference period in the Climate Atlas are from the authoritative statistics, which are provided by the Kystdirektoratet (KDI, see Section 6.2). KDI provides the authoritative statistics reports for ESLs in Denmark, and is updated approximately every five years with the latest one published in 2017 and revised in 2019 [Ditlevsen et al., 2019]. The storm surge water statistics are based on measured water levels at tide gauge

stations along the Danish coasts (67 stations in the 2017 report) with a sufficiently long time-series. The 2017 statistics report, which is used for Climate Atlas, includes measurements until the beginning of 2017. For individual stations, different statistical methods are applied, giving an assessment of how frequently extreme water levels are to be expected.

A storm event can last for a short period of time or extend over several days. Several high water events can therefore be related to the same storm event. In this case, only the highest measured water levels recorded at the individual sites are treated as extreme water levels, and in order to ensure that the extreme water levels are independent a 36-hour criteria is applied. Such a principle is also adopted for the climate simulations.

For the return levels not included in KDI statistics, we applied certain methods to extrapolate KDI statistics (discussed in Section 6.2). For coastal planning and climate adaptation, please note that these return levels under present climate should be used with caution, and should always be combined with a expert analysis of the local conditions. The major focus of the Climate Atlas project is to understand the influence of the anthropogenic climate change and provide a dataset to support coastal climate adaptation strategy. There is little evidence that storm changes influencing Denmark (extratropical cyclones) in the past could be attributed to anthropogenic climate change (see the detailed discussion in Oppenheimer et al. [2019]). Therefore, the implementation of the KDI statistics for the coastal planning today should remain. The following sections will discuss how we consider storm surge statistics under the future climate change scenarios.

6.1.2 Why will storm surge heights increase?

Flood risk is exacerbated due to its interaction with the SLR. In Church et al. [2013b], ESL increase with SLR was marked as *very likely*. However, it was noted as *low confidence* in region-specific projections, as there was limited number of studies and a poor geographical coverage before the publication of AR5.

Since then, many datasets have become available, e.g. the Global Extreme Sea Level Analysis [GESLA-2 Woodworth et al., 2016]. Oppenheimer et al. [2019] concluded with *high confidence* that the inclusion of local processes is essential to estimate local changes in ESL. Thus, a thorough analysis of the local impact of winter storms is a prerequisite for a reliable local storm losses trend (the storm losses refer to the heavy damage of infrastructure and environment, restriction to traffics and injury or even loss of lives) [Donat et al., 2010].

Donat et al. [2011] investigated multi-model simulations from global (GCM) and regional (RCM) climate models, and found that extreme wind speeds will increase by up to 5% over northern parts of Europe in most simulations. We also made some investigations for several stations in Denmark using EURO-CORDEX members (see Section 6.2.2). It is hard to draw any conclusion from the current investigation, and further studies are necessary and planned for the next releases of the Climate Atlas.

6.1.3 Scope

The 2019 release of the Climate Atlas focuses on ESL events with statistical return periods (Section 4.2) of 20 and 50 years. Return periods have an inverse relationship to the average frequency of occurrence. Therefore, water levels corresponding to the 20 and 50 year return levels have a respective probability of 0.05 and 0.02 of being exceeded in any given year.

The 2020b release of the Climate Atlas focuses on the estimation of extreme water levels with a lower probability of occurrence, i.e. 100 and 10000 year return levels. In addition, return levels of 1 year and 5 year events are also estimated, as well as the future frequency of current 20 year events. The methods are partly illustrated in Figure 14, with more details in Section 6.2

6.1.4 Hydrodynamic modelling for extreme sea level studies

The ESL intensity change in the future can be estimated with statistical models or hydrodynamical models. The advantage of using hydrodynamical models is that they can quantify interactions between the different components of ESL [Arns et al., 2013]. The important meteorological input for ocean models are wind speed and direction, and sea level pressure. From a global reanalysis data-set, modelled and observed sea level agreed quite well (with RMSE $<$ 0.2 m) over the reference period 1980-2011 [Muis et al., 2016]. However, it is still a challenge when running these models in climate mode because of inherent limitations of the climate projection data, e.g. resolution, precision and accuracy.

6.1.5 Challenges of sampling

The Climate Atlas model simulations are divided into time slices of 30 years. We use extreme value analysis (Section 4.2) to estimate the probability of events which occur on average less often than once within this period. The estimations are based on an implicit assumption of stationary statistics. Since each extreme events have a low probability of occurrence in any given year, but are here assumed independent, it is possible for several low probability events to appear by chance within a 30 year time slice. Occurrences of low probability events within this period will bias the return period towards low values. On the other hand, absence of low and moderately low probability events will result in a bias towards higher return periods. This sensitivity to the sampling period can be reduced by increasing the length of the sampling period, but this is a trade-off, since climatic stationarity in the sampling period is implicitly assumed.

6.2 Methods

6.2.1 Budget of storm surge changes

The climate historical simulation should be bias-corrected to the observations. For the uncoupled ocean simulations, one could apply the bias correction for the atmospheric forcing using

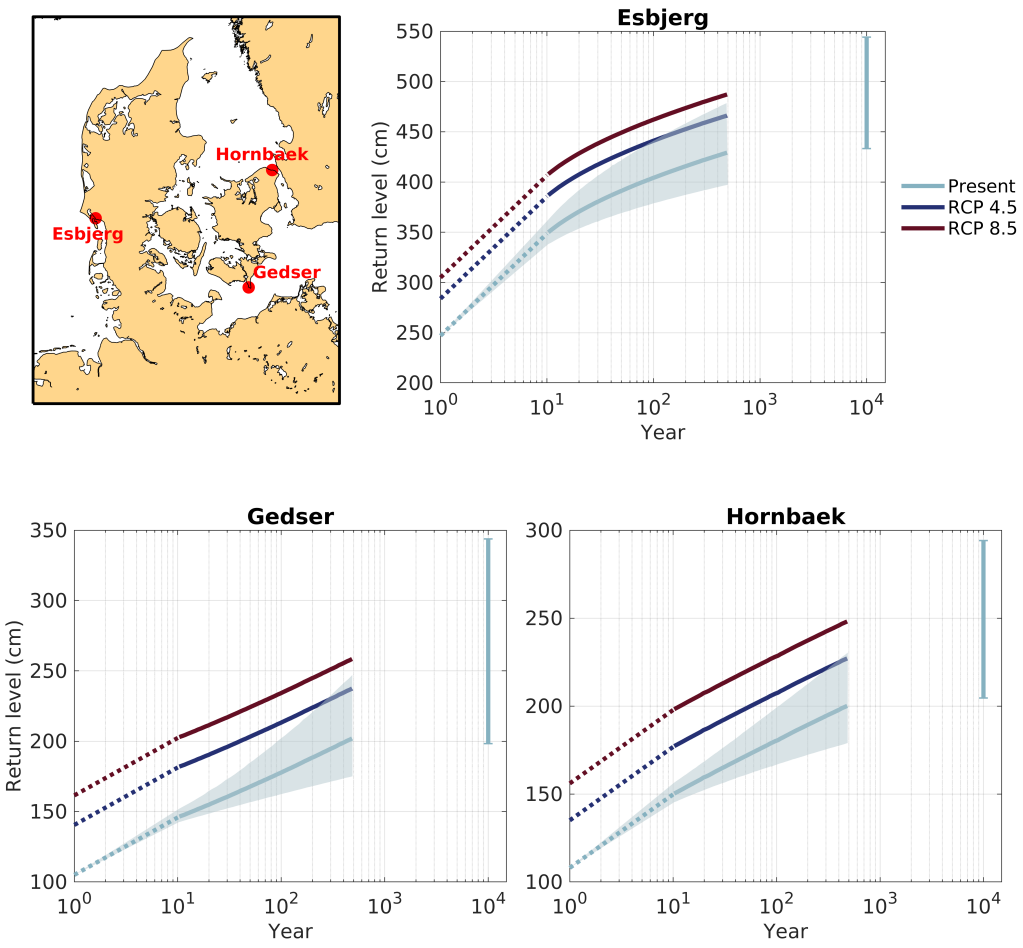

Figure 14: The expected extreme sea level (ESL, cm) at the end of this century with the corresponding return period on x-axis at the locations of the three oldest tide gauge stations in Denmark (locations are marked in the upper-left panel). The plots are comparing the present day values (grey) and the future conditions (RCP4.5 and RCP8.5 scenarios, in blue and red, respectively). The grey solid lines are based on tide gauge observations, and the grey bands refer to the 5–95% uncertainty range in the fit of the extreme value distribution to observations from Ditlevsen et al. [2019]. The dashed lines refer to the linear interpolation of the logarithmic return-time between 1 year and 10 year events. The error-bars indicate the uncertainty range for the extrapolated 10,000 year events under present climate.

adjust-mean methods. The adjust-mean methods allow to keep the variability of the climate model, while the climatology is adjusted to the observations. However, it is inappropriate to bias-correct the wind direction and pressure system [Mathis et al., 2013]. Hence, for the storm surge study, we have not seen bias-correction for the forcing as an appropriate way.

In Climate Atlas, we applied the 'delta change' method (Section 2.2) for the estimation of future storm surges. This means that we use observations for the present day values directly instead of bias correcting the model results. The future change of the storm surge statistics is directly added to the observed statistics. Another argument for the benefit of this method is that it facilitates the use of the KDI statistics. The KDI statistics should be kept since it is the authoritative storm surge statistics based on long-term observations, and to minimise the effect of the sampling problem mentioned in the last section.

However, for Climate Atlas release 2020b, KDI statistics 2017 did not provide the 1, 5 and 10000 year return levels. Thus we applied interpolation/extrapolation methods to the KDI statistics as shown in Figure 14. KDI statistics 2012 [Sørensen et al., 2013] provided 1 year return levels, which are directly used after evaluation. Thus, 5 year events are interpolated using 1 year and 10 year return levels. For 10000 year return levels, considering the large uncertainty for stations with observational records of less than 100 years, we only release data for the coastal stretches containing the 11 stations with records longer than 100 years in Climate Atlas release 2020b. For those 11 stations, we applied a linear extrapolation method of the logarithmic return-time. Moreover, further evaluation of the estimated 10000 year event is conducted based on other datasets, including statistical methods different from the KDI statistics, hindcast model simulation results and model-based artificial extreme wind experiments. The references for those datasets will be updated with Climate Atlas release 2021.

The algorithm for calculating storm surge change is described in section 8.2.3.

6.2.2 Simulations of wind-generated component

As described in Section 5.2.1, we employed a limited number of EURO-CORDEX members for the storm surge modelling in the Danish Climate Atlas project. The extreme wind from different RCMs differ from member to member and place to place. To provide a general picture of how the extreme wind in these two members differ from ensembles, we illustrated the time series of annual maximum wind speeds (AMWS) at two representative stations (Esbjerg and Hornbæk, Figure 15). At Esbjerg station, the AMWS in HIRHAM5 showed about 10 $\mathrm{m\,s^{-1}}$ higher than ensemble, while the AMWS in RCA4 was closer to ensemble median values. We can draw very similar conclusions for the AMWS time-series at Hornbæk station. This investigation focuses on annual max wind speed only, whereas studies of storm tracks and related changes in wind direction and duration are left for the future.

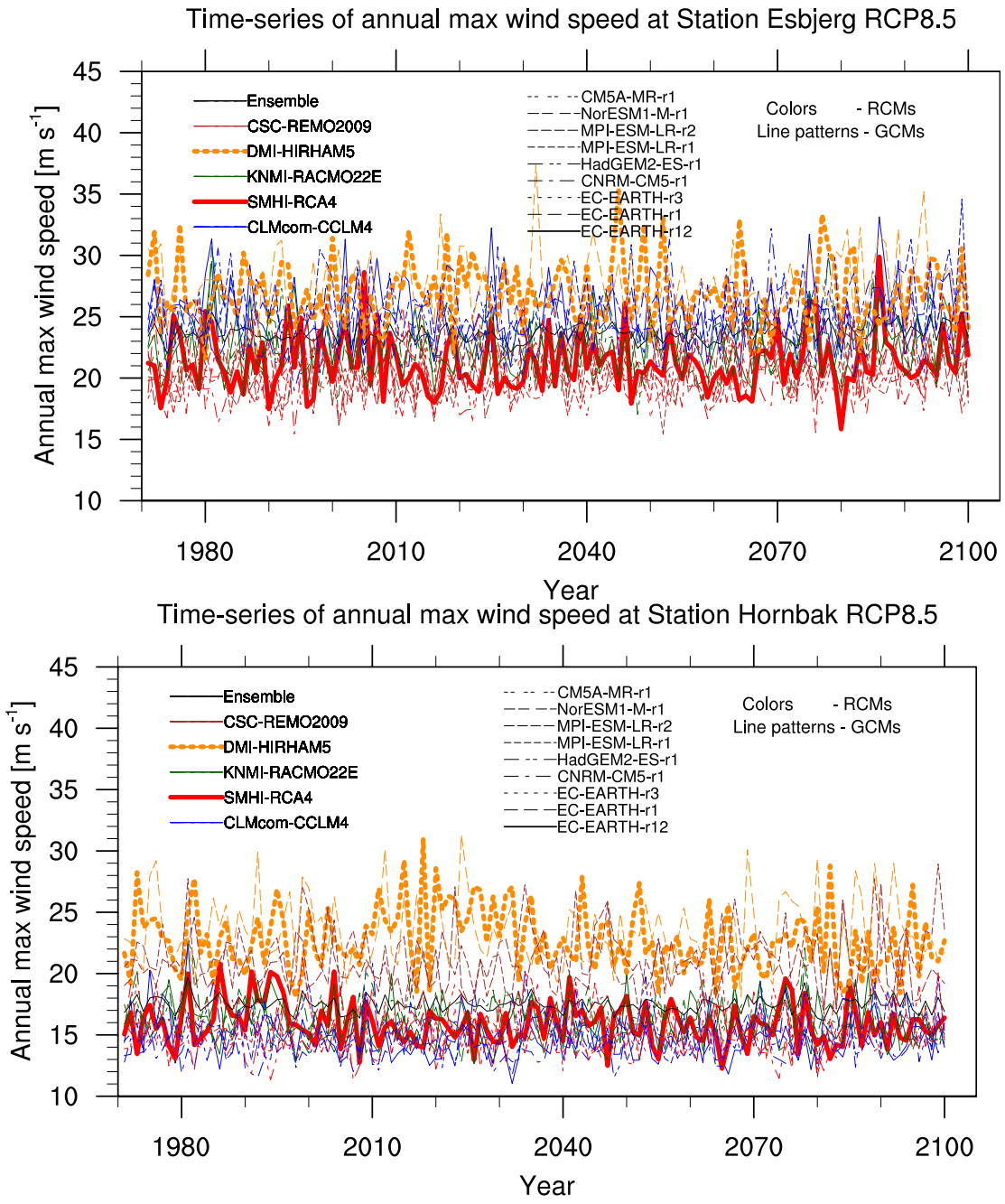

Figure 15: Time series of annual maximum wind speed (m s^{-1}) at the station Esbjerg (upper panel) and Hornbæk (lower panel). The time series are 130 years results from multi-RCM (16 members, including 5 RCMs: REMO2009 with 2, HIRHAM5 with 2, RACMO22E with 3, RCA4 with 5 and CCLM with 4 members) simulations under RCP 8.5 scenarios. The line colours indicate different RCMs, while different line patterns refer to GCMs (downscale to RCMs). DMI-HIRHAM5 and SMHI-RCA4 used in the current release are single dashed thick yellow line and thick red line respectively.

6.2.3 Statistic methods for wind-generated component

To keep the consistency with other indexes in this report, we used POT and GPD methods to generate the storm surge return values (same parameterized extreme-value procedure is used as that described in Section 4). In POT methods, 30 events over the 30 year period were used as the threshold. However, there are two notable differences with other indexes in the current release. First, we are using the KDI statistics for the present day climate simulations, so the return value fitting methods for present day follow the definition from KDI (see 6.2). Second, for the uncertainty estimates, one assumption has to be made since we only used two ensemble members, i.e. the difference between two ensemble members should be smaller than the uncertainty range estimated by KDI present day statistics to guarantee the exclusion of the outliers.

To combine the uncertainty of storm surge and SLR, root squared methods are applied. However, for the rare storm surge events in release 2020b, we only consider the uncertainty of SLR for 100 year and 10000 year events, since 30 years slice is too short to estimate the low probability extreme storm surges. We further ensure that the e.g. 100 year return values are larger than 50 year return values and that they in-turn are larger than 20 year return values for both 10- and 90 percentiles.

6.3 Results

The extreme water level is an exceptional high water level, which occurs rarely and is caused by special wind and weather conditions. Depending on the locations, a big difference is expected when a water level can be characterised as an extreme. In Denmark, the biggest variation is found in the Danish part of the Wadden Sea, where extreme water levels can reach between 4 and 5.5 meters. Along the Kattegat coasts, extreme water levels over 2 meter are rare. Extraordinarily high water levels occurred as a result of strong storm wind and characteristic patterns of low and high pressure systems over Northern Europe, e.g. during Bodil storm Dec 2013. Such a strong storm event can also influence part of the Danish Straits (Danish: Bælterne), while the stations along the southern Baltic Sea coast are more influenced by Baltic type of storm.

With the methods described above, the best estimates of changes in 20-, 50-, 100- and 10000-year storm surges follow those of the mean sea level (see Section 5.3). The uncertainty range varies from one coastal stretch to the next, and depends on both the uncertainty of the observation-based present day statistics, the hydrodynamic model simulations and the mean sea level rise uncertainty. All values are available in the online Climate Atlas.

7 Uncertainties

A data-product like the Climate Atlas should not only give the magnitudes of numerical quantities, but also the *uncertainties* coupled to these quantities.

Cloudbursts, for instance, are likely under-observed since the events are small in extent and rare. Limited lengths of records have their main impacts through sampling of the climate-variability: The climate system affecting Denmark has low-frequency variability and sampling such a sequence of data with limited-length windows causes a sampling issue: we may have samples from the real climate that are not representative of the mean climate. For instance, the North Atlantic Oscillation is a phenomenon influencing the track of low pressure systems in the North Atlantic. Therefore, temperatures, precipitation and winds over Denmark are dependent on the state of the NAO index. The influence of this is sampled by the limited availability of calibration-data.

At the moment, our understanding of the uncertainties is based on the spread provided by the models which we have available. Additional sources of uncertainty follow from the use of scope-limited observational material and from the use of interpolations and gridding techniques.

A good way to probe the relative importances of these sources of uncertainty, is to apply resampling of the data used, and re-parametrizations of the methods used. In 2019 we have employed resampling of observational data and the models used; in the future we will also probe the dependency on methods.

To perform the resampling of data we employ 'bootstrapping with replacement'. We apply the method to the years for which observational data exist, and for the models used. We do it separately so that the effects of these two important factors can be isolated.

The procedure is straightforward and is mainly one of repeating the calculation of the climate atlas indices under random picks of years or models, followed by collation of results. We simply look at the spread - standard deviation - in the main result we report on: the 10, 50 and 90%-iles themselves. We report results for the end-of century period and for the RCP8.5 scenario, as we expect the largest effects there.

In Table 10 we show the standard deviations of the percentile levels reported on in this report (i.e. 10, 50 and 90). We are sampling local anomalies in order to exclude the considerable effect of goegraphic variations.

The Table is complex to interpret quickly and we have put it at the end of this report so that unwarranted confusion does not arise upon encountering the table in the main text. A brief explanation of what is in the table follows, *but the reader mainly interested in following the flow of the text may wish to skip the rest of this paragraph*: For each index, and for either bootstrapping observations (label S1 at head of column) or models (header S2 on column) we give 4 numbers — these are on two lines and each pair is separated by a semi-colon. On the *first line* and *in front* of the semi-colon is given the largest (i.e. 'worst-case') standard deviation of any of the percentiles 10, 50 and 90 for absolute values in the climate index. On the first line

after the semi-colon is the largest standard deviation for any of the 10, 50 and 90%-iles of the *change* in the index. On the *second line* is given the same information as in the first line but now *only for the median* (i.e. the 50%-ile). We split the results in this way with the expectation that the effect on percentiles might not be the same for the 10, 50 and 90%-iles given small number statistics.

We did not apply bootstrapping on the climate indexes dealing with sea-levels and storm surges as the uncertainties there are given by error-propagating due to the limited number of sea level models currently available. In the future we could also probe the ocean-indices' uncertainties by resampling means.

So far, only 9 bootstraps have been performed, and only partially on factors S1 and S2. However, these first results allow some general conclusions.

We see some differences in the effects of bootstrapping S1 (observation years) and S2 (models), respectively: For index 001 and 106, the effects due to bootstrapping on S1 and S2 are about the same for the absolute values and the climate signals in these (i.e. their changes over time). For indices 101-105 the standard deviation in the climate change signal is much bigger for S2 bootstrapping than it is for S1 bootstrapping.

For indices 107 and 151-162 we only have results for S2 bootstrapping. Here we note that the standard deviation on the climate signal for 151-162, due to S2 bootstrapping, is in the range 5-16%.

107 has very small response to bootstrapping, it appears.

Only minor differences are seen throughout when comparing standard deviations induced by bootstrapping for any of the percentiles 10, 50 and 90 when just considering the 50th percentile.

In **summary**:

- choice of models has greater influence than the choice of calibration period, by factors of from 4 to 10 (indices 101-105)
- uncertainties due to model choice can reach 16% in the change of indices related to extreme precipitation
- robustness of the 10, 50 and 90th percentiles to S1 (observation years) and S2 (models) bootstrapping are similar.

We should thus seek to extend the number of models used, and we should accommodate an analysis of the importance of calibration period position in time which could not be sampled by the present bootstrap analysis. More and longer observed data series should be obtained.

Extending the number of factors considered in bootstrapping could provide us with an important tool for calculating 'total uncertainty' on the climate atlas information.

7.1 RCP4.5 error bars

The number of RCP4.5 models is about a factor of 2.5 less than for RCP8.5 and this leads to unfortunate effects due to small sample size and model inter-correlations (the few mod-

els present are somewhat dependent). The error bars for RCP4.5 results therefore show a tendency to vary a lot between future time periods, as well as, now and then, having unrealistically small widths. This prompts us to apply an adjustment scheme so that we can present estimated error bars for RCP4.5 results that are realistic.

We ensure that

1. The RCP4.5 error bars in near future and mid-century are adjusted so that the smaller one is scaled to the width of the larger one, and
2. the end of century error bar is scaled so that it is never the smallest of the three error bars.

The scaling algorithm applies a factor on the error bars, when scaling is called for, which retains the ratio of the upper (50 to 90 percentile interval) error bar to that of the lower (10 to 50 percentile) error bar, while keeping the median value fixed.

A larger ensemble of models would remedy this problem from the root, but the EURO-CORDEX ensemble of models is limited in scope for the RCP4.5 scenario.

8 Implementation details

8.1 Land areas - municipalities and main catchment areas

The detailed implementation of the calculation of each index is given in the following.

For each index calculations proceed as follows: Annual and seasonal mean (or also max/min, depending on the nature of the index) values are calculated at each EUR-11 grid-point from daily-mean model values. This gives 30 annual values for each of the chosen reference (historical and scenario) periods we have chosen. The mean of the 30 values is then taken. Then differences between historical and future periods are calculated for indices requiring relative changes. Then re-gridding and smoothing is applied to relative changes and absolute values to attain a smooth 1x1 km grid. 10, 50 and 90 percentile values are determined from these values.

8.1.1 Models used

The models we use from the CORDEX archive is a subsample of what is available. Not all of the CORDEX models are comparable: CNRM version 1 models used the incorrect boundary forcing and were excluded. Despite using a differently rotated grid, the Aladin model has been re-gridded to the EUR-11 standard grid, and is used. Table 7 and 8 list the models actually used.

8.1.2 Grid transformations

Interpolation is performed linearly to render the index values onto a 1x1 km grid ('det Danske Kvadratnet') from the EUR-11 grid of the models. The interpolation uses **matlab** routine *scatteredInterpolant* which uses a Voronoi triangulation of the scattered sample points to perform interpolation. Natural neighbour interpolation is used via the "natural" option [Sibson, 1981]. Further implementation details for the *scatteredInterpolant* routine is given at Mathworks [2019].

8.1.3 Smoothing

Smoothing of the resulting 1x1 km grid is performed to avoid unrealistic details. We smooth all fields, after interpolation, by taking averages over moving box-windows of size 25×25 km. Since observed spatial structure is more credible than modelled future spatial structures in changes, we smooth the projections spatially with a bigger (75x75 km) filter, before calculating index changes (exception for winds, see Section 8.3).

Details on 'det Danske KvadratNet' are available at Danmarks Statistik [2019].

For each index relative as well as absolute values of the expected values of the period-mean quantities are calculated. For relative changes we use the historical reference period

1981-2010, and the future periods 2011-2040, 2041-2070 and 2071-2100. These future periods are also used when giving the absolute values. The 10, 50 and 90 percentiles are calculated from the differences between the mean values over reference vs. scenario periods for each available model. The percentiles thus illustrate *model-spread*.

The boundaries for municipalities are defined by Styrelsen for Dataforsyning og Effektivisering (SDFE) and as this product can be updated we state here that the information was downloaded in May of 2018. Future updates by SDFE are bound to be have very minor impacts and are typically incremental when, typically, water-bodies (streams) and beach-lines change. See SDFE [2019].

The boundaries for Main catchment areas are given by Miljøstyrelsen [MST, 2019].

The boundaries used for Coastal stretches are discussed below in section 8.2.

8.1.4 Generic procedures

We next describe generic procedures for calculating area-specific absolute or relative-change indices for the temperature-like quantities in the Atlas (index 001), the precipitation indices (101-106,108-109, 151-162) and the cloudburst index (107). We will refer to these procedures when describing each index and note any deviations from the procedure, for completeness sake. Generic Procedure 1 deals with index 001 and 101-106. Generic procedure 2 deals with 151-162 and 201-203, and Generic Procedure 3 deals with index 107.

8.1.4.1 Generic Procedure 1: For means and not very extreme indices

The following is the procedure specifically for temperature in land-areas such as municipalities and catchment areas, and the precipitation indexes.

1. Regridding of observational data to the CORDEX grid

   For all model grid points with at least 50% land coverage the nearest KGDK grid-point is found, and this 'nearest neighbour' time series is used as the assigned observational data point for that model grid point. We use nearest neighbour method, rather than interpolation, to avoid any smoothing of data implicit in most interpolation methods. Distance is calculated in the straight line - no great-circle calculation is performed. We determine whether the model grid cell has at least 50% land by inspecting the same grid-cell in the model land-sea mask. To ensure that small islands, for which the land-sea mask may indicate less than 50%, we specifically assign ls-mask values above 50% so that the data at the island have appropriate weight. This was done for Anholt and Læsø.

2. Bias Adjustment

   For each model, and for each of the 4+1 seasons, the 99 separate percentiles are determined for the observed data and for the model by interpolation in the assembled values. A robust linear regression is then performed using the 99 data-pairs, and the slope of the regression line is noted. The slope is used to linearly extend the 99-point

sequence beyond its range - to higher and lower values. See Figure 3 for an illustration of the procedure. The linear extensions are made starting in the last and first points of the sequence with the previously noted slope. On scenario data a quantile-quantile transformation is now performed using this constructed relationship. It is based on linear interpolation between points on the 99-pair percentile sequence if the interpoland (that is, the scenario value) is between the max and min of the sequence ordinate. If the interpoland falls either above or below the max and min of the ordinate range the linear extensions are used. The **matlab** robust regression routine is '*robustfit*'. When the 4 seasons have been completed, the results are combined to provide the annual time series.

3. Index calculation

   For each year, and each of the 4+1 seasons, and for each CORDEX model grid-point, in each model we calculate the index in question using the bias-adjusted data. Split the results into the 30-year long reference and future scenario periods (some models only have 29 years of data in the last of the future periods, and some end in November of the last year). Take means over the 30 values in each period, at each grid-point, and for each season etc. Calculate changes in indices (differences or ratios, in %, as appropriate, and noted for each index below) between the future periods in question and the reference period.

4. Regrid indices to the KGDK 1x1 km grid.

   Use the **matlab** routine '*scatteredInterpolant*' with option '*natural*'. This 'smooths the result' into neighbouring cells to a small degree. The 1x1 km land-sea mask is applied to remove apparent values over sea points.

   Smooth the observed results with **matlab** routine '*smooth2a*' using square 25x25 km windows - the window moves in 1-km steps; smooth projections for the future with 75x75 km windows.

5. Ensemble averaging

   For each 1x1 km grid-point collect the 57 model-index values relevant for the season and extract the 10, 50 and 90 percentiles, using the **matlab** routine named *"prctile"*[4], which *interpolates* in the values presented to it. This grid is one end-product for the homepage.

6. Area-aggregation

   For each municipality or main catchment area, identify the 1x1 km grid-points inside the boundary polygon - i.e. find all grid-points with centre-coordinate inside the given polygon. Calculate the mean of the 10, 50 and 90 percentile data generated above. This product is another product for the homepage.

[4]Used with implicit argument 'exact'.

8.1.4.2 Generic Procedure 2 - for extreme events

This procedure is used for rare precipitation events, except cloudbursts (see Generic Procedure 3 for that)

1. Recreation of Spildevandskommiteens NRM model (see [Gregersen et al., 2014b]). This results in a 10x10 km grid (on 'det Danske Kvadratnet') of the λ-parameter (number of exceedances of the threshold per year) and the scale-parameter for a generalized Pareto distribution. Both for 1-hour data and 24-hour data.

2. For the calibration-period and the reference as well as the three future periods, for land points only, for RCP4.5 and RCP8.5, we apply nearest-neighbour interpolation from the CORDEX model grid to the 10x10 km grid. The nearest-neighbour interpolation assigns the model series in the nearest CORDEX gridpoint to 'det Danske Kvadratnet' point under consideration.

3. Perform extreme value analysis for all models and the calibration period and all scenarios, and 1 and 24-hour data. 24-hour analysis performed with sliding windows covering 24-hours but advancing one hour each step).

   For lower and lower thresholds find model points exceeding the threshold until $\lambda = 3$ (events/year) is found (this will be a different threshold for each model, period and landpoint, but all with $\lambda = 3$. Ensure at least 24 hours between each selected event.

   Fit a generalized Pareto distribution to the selected values, using the probability-weighted method. Thereby find local scale and shape parameters.

   Average the shape parameter to one national value.

   Calculate return-levels from the GP parameters for the calibration-period.

4. use the parameterized *q-q* transformation (see section 4) to correct the return-levels of the calibration period.

5. In the reference-period and the three future periods correct the return-levels using the parameterized *q-q* transformation determined in the calibration period (with Equation 9).

6. Files with *q-q* corrected return-values are prepared for the reference-period and the three future periods, for the next processing steps - i.e. Generic Procedure 1, steps 4-6.

8.1.4.3 Special version of Procedure 2 - for cloudbursts

This procedure is used for cloudbursts but follows closely the method laid out for GP2, above. Since the models only have hourly data, and a cloudburst is defined as 'more than 15mm of precipitation in 30 minutes' we employ a simplified scaling method. From observations [Cappelen, 2017] we know that on a national observational system of about 258 measuring stations (numbers vary from year to year, the 258 average is for the 2011-2018 period), on average 87 cloudbursts were observed. That is, at each station on average you have to wait 3 years to observe a cloudburst.

1. Determine, in each gridpoint of each of the 1-hour precipitation models (see Table 8 for the complete list of model names) placed on 'det Danske Kvadratnet' grid, the event-level that occurs every three years.
2. For each model and each time period, use the relevant parameterized *q-q* transformation to convert the level determined in 1, to the return period.
3. Put gridded return periods into files for the next steps.
4. Finish with Generic Procedure steps 4-6.

8.1.4.4 Special version of Procedure 2 - for temperature maxima and minima and the daily temperature range

We discovered that the model-fields for temperatures, their maxima and their minima – which are delivered from CORDEX as separate files generated by the individual contributors – did not all fulfil such basic requirements as $T_{min} < T_{mean} < T_{max}$. So before starting the bias adjustment procedure for modelled daily minimum and maximum temperature, we made corrections for each model, each day and each grid cell so that T_{min} is given the lowest value of T_{min}, T_{mean}, T_{max}, and T_{max} is given the highest value of the three variables and T_{mean} is given the middle value of the three. The daily maximum and minimum temperatures were bias adjusted together rather than separately as with daily mean temperature using the steps below. The daily mean temperatures were QQ-scaled against gridded observed data from KGDK at a 20x20 km resolution for the period 1989-2019 using the GP2 procedure already described.

- The modelled daily temperature range ($DTR = T_{max} - T_{min}$) was QQ-scaled against gridded observations for the period 2011-2019, resulting in DTR_{BA}. All instances were $DTR_{BA} < 0$ were set to 0.
- The skewness $Z = T_{mean} - (T_{max} + T_{min})/2$ was calculated for model data and then QQ-scaled against gridded observations, resulting in Z_{BA}.
- Then bias adjusted T_{min} and T_{max} were calculated using the equations $T_{min,BA} = T_{mean,BA} - Z_{BA} - DTR_{BA}/2$ and $T_{max,BA} = T_{mean,BA} - Z_{BA} + DTR_{BA}/2$.

The KGDK data for daily maximum and minmum temperatures used here is limited to the period 2011-2019. In 2011, a change in observing praxis occurs: before end of 2010 data were recorded from 6AM to next 6AM, but after start of 2011 it was recorded midnight to midnight. While T_{max} is very likely always recorded at a cadence of one day, we suspect that T_{min} may be recorded with occasionally unpredictable offsets of one day in the older system of recording because the coldest time of day is usually in the morning hours - sometimes before 6 AM, sometimes after - thus producing the larger variation in Z before end of 2010. This problem effectively limits us to use data after the start of 2011 for indexes involving bias-adjusted temperature maxima and minima. See Figure 16.

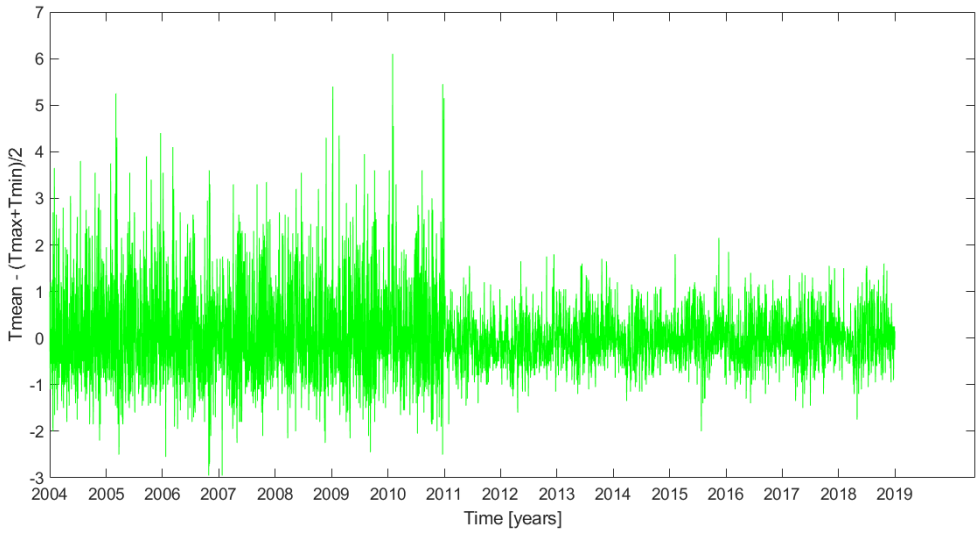

Figure 16: The skewness ($Z = T_{mean} - (T_{max} + T_{min})/2$) of 20x20 km gridded KGDK maximum and minimum temperature data changes at 2010/2011.

8.2 Implementation details for ocean indices

The detailed implementation of the calculation of ocean indices is given in the following.

8.2.1 Coastal stretches

The ocean indices are calculated for the 36 coastal stretches defined by KDI, except Ringkøbing Fjord and Nissum Fjord, which are regulated by lock gates (Table 6, KDI code VK2 and VK3). Each coastal stretch is represented by one station (Table 6), chosen to have the most reliable present day high water statistics for the coastal stretch. The mean sea level rise information and the hydrodynamic model results are interpolated to these stations using a nearest neighbour approach. Note that for 10000 year extreme sea level indices, the length of the observed tide gauge time-series in some stations are too short to perform extreme value statistical analysis. Hence, these values are only included where the time series are sufficiently long (as described in Section 6.2).

The uncertainty intervals of the extreme sea level indices (202, 203) for the Limfjord (LF1, LF2, LF3 and LF4) have been calculated without expansion of the uncertainty interval based on hydrodynamic model simulations in the current Climate Atlas, since the hydrodynamic model for the Limfjord was not available for the study. They require separate simulations of a nested Limfjord model domain, which may be include in future Climate Atlas updates.

8.2.2 Hydrodynamic model used

DMI operates the regional 3D ocean model HBM (the HIROMB-BOOS Model) for the North & Baltic Seas, in order to provide forecasts of the physical state of the Danish and nearby waters five days ahead [Berg and Poulsen, 2012, Fu et al., 2012]. We employed this operational model to perform the climate simulations. The DKSS operational setup (details on `http://ocean.dmi.dk/models/hbm.uk.php`) with the nested high-resolution inner Danish water domain was selected for the Climate Atlas project (model version HBM-2.8). The use of operational models for climate studies allow the same level of details in the climate projections as in the operational setup used for ocean forecast, and guarantees a well-tested and validated system. The validation of the storm surge forecast includes online validation and case studies can be found on `http://ocean.dmi.dk/validations/surges/index.uk.php`.

8.2.3 Implementation steps for storm surge indexes

1. Three CORDEX members was selected to perform the transient climate simulations (refer to Section 6.2.2).
2. We used the DMI storm surge operational model to derive the projected extreme sea levels (details in Sections 8.2.2 and 5.2.1).
3. Instead of bias-correcting the historical climate simulations, the KDI statistics were directly used for the present day/historical the storm surge indexes (Sections 6.2.1). Note that, obtaining 10000 year return levels requires extrapolation from the KDI statistics.
4. Using the two transient climate simulations to derive the uncertainties of the future storm surge change due to extreme wind change (Sections 6.2.3).
5. The uncertainties in SLR is root square added to the uncertainties of wind induced storm surge change. However, for 100 year and 10000 year return levels we only consider the uncertainties in SLR.

Table 6: The names of the 36 coastal stretches and the observing stations that represent the coastal stretches. The KDI code is the name of coastal stretch following the KDI definition. *VK2 Ringkøbing Fjord and VK3 Nissum Fjord are not included in the Climate Atlas, as the water level in the two fjords are regulated by lock gates.

KDI code	Name for coastal stretch	Name for stations
VH1	Vadehavskyst sydlig	Vidå
VH2	Vadehavskyst central	Ribe
VH3	Vadehavskyst nordlig	Esbjerg
VK1	Vestkyst central	Hvide Sande
VK2*	Ringkøbing Fjord	
VK3*	Nissum Fjord	
VK4	Vestkysten ud for Limfjorden	Thyborøn
VK5	Skagerrakkyst sydlige	Hanstholm
VK6	Skagerrakkyst nordlig	Hirtshals
LF1	Limford østlig	Nr. Sundby
LF2	Limfjorden ved Skive	Skive
LF3	Limfjorden ved Lemvig	Lemvig
LF4	Limfjorden ved Thisted	Thisted
OJ1	Kattegatkyst nordlige	Frederikshavn
OJ2	Ålborg Bugt	Hals Barre
OJ3	Randers Fjord og Mariager Fjord	Randers
OJ4	Djurslands østkyst og Anholt	Grenå
OJ5	Århus Bugt	Århus
OJ6	Lillebælt nordlig	Juelsminde
OJ7	Lillebælt central	Fredericia
SD1	Lillebælt sydlig	Fynshav
SD2	Sydfynske Øhav	Fåborg
SD3	Storebælt Sydvest	Slipshavn
SD4	Femern Bælt	Gedser
SD5	Smålandsfarvandet	Karrebæksminde
SD6	Falsters og Møns Østersøkyst	Hesnæs
SD7	Faxe Bugt	Rødvig
SJ1	Storebælt nordvest og Odense Fjord	Kerteminde
SJ2	Storebælt nordøst	Kalundborg
SJ3	Sejrø Bugt	Ballen
SJ4	Nordsjællands kyst	Hornbæk
SJ5	Isefjord	Holbæk
SJ6	Roskilde Fjord	Roskilde
SJ7	Øresunds kyst	København
SJ8	Køge Bugt	Køge
SJ9	Bornholms kyst	Tejn

8.3 Notes on Individual indices

The index numbers refer to Table 1.

- **001 Mean temperature** is entirely based on Generic Procedure 1. The complete list of CORDEX models used for this index are given in Tables 7 and. The observational data used to bias-adjust against, for this index, is taken from Klimagrid Danmark, with time coverage from 1989 to 2018, and with a spatial resolution of 20×20km. The time-resolution of this dataset is daily. The actual files accessed are given in Table 8. Two datasets are provided for Klimagrid Danmark - the first covers 1989-2010, and the other covers from 2011-2018.
- **002 Daily maximum temperature** The model data-set for daily maximum T is bias-corrected against Klimagrid Danmark gridded values. Daily KGDK data on the 20x20 km grid are used, covering the years 2011-2019.
- **003 Daily minimum temperature** The model data-set for daily minimum T is bias-corrected against Klimagrid Danmark gridded values. Daily KGDK data on the 20x20 km grid are used, covering the years 2011-19.
- **004 Highest temperature** The model values for seasonal/annual highest temperatures are bias-corrected using QQ-scaling against the KGDK observed values of that quantity, and the bias-corrected values averaged over the 30 years.
- **005 Lowest temperature** "Generic procedure 4" (a special version of GP2 implemented to deal with specific model-related problems regarding temperature maxima and minima (See section 8.1.4.4 for details)
- **006 Annual temperature range** Generic Procedure 1.
- **007 Diurnal temperature range** Generic Procedure 4
- **008 Heat-wave days** Generic Procedure 4
- **009 Warm-wave days** Generic Procedure 4
- **010 Frost-days** Generic Procedure 4
- **011 Growing season length** Generic Procedure 1.
- **101 Mean precipitation** Like Generic Procedure 1 in section 8.1.4.1, but with these exceptions:

  1. Regridding, observational data based on the Klimagrid Danmark (KGDK) dataset with a spatial grid 10x10 km, and coverage is 1989-2018.

  2. Bias Adjustment, before application of the BA algorithm all zero values are set to a small random number between 0 and 10^{-12} in model and observations; after BA all adjusted model numbers smaller than 0.1 are set to zero.

3. Index calculation, the relative change in percent is calculated.

4 - 5 - 6. The same as in Generic Procedure 1.

- **102 Daily max precipitation.** Just like index 101 but the mean of the 30 annual maxima (or annual series of seasonal maxima) is taken.
- **103 5-day max precipitation.** A 5-day window is moved along the precipitation time-series and the sum over the 5 days calculated and noted against the centre day of the window. This means that 2 days at the start and 2 days at the end are lost. Then the maximum values of this series for the relevant 4+1 seasons etc are determined.
- **104 14-day max precipitation.** Just like index 103, but instead of a 2+1+2 day window a 6+1+7 day window is employed.
- **105 Days with more than 10 mm precipitation in a day.** A count is made of the number of days with more daily precipitation that 10mm, for the relevant 4+1 seasons, etc. That gives 30 annual counts which are averaged.
- **106 Days with more than 20 mm precipitation.** Just like index 105, but for 20 mm precipitation.
- **107 Number of cloudbursts.** The number of cloudbursts per year are derived from the parametrised EVD for future periods given the current rate of observed cloudbursts.
- **108 Number of dry days** Number of days of the year or season with precipitation below 1 mm.
- **109 Maximum dry spell length** Length of the longest period of the year or season with consecutive days with precipitation below 1 mm
- **151 hourly precipitation of events with 2-year return period (in mm/hr)**. From the *q-q* scaling steps described in Generic Procedure 2 (see also Section 4) we have essentially maps for each model and each period and each scenario of the bias-corrected return-levels.
- **152 hourly precipitation of events with 5-year return period (in mm/hr)** As index 151 above but for 5-year events.
- **153 hourly precipitation of events with 10-year return period (in mm/hr)** As index 151 above, but for 10-year events.
- **154 hourly precipitation of events with 20-year return period (in mm/hr)** As index 151 above, but for 20-year events.
- **155 hourly precipitation of events with 50-year return period (in mm/hr)** As index 151 above, but for 50-year events.

- **156 hourly precipitation of events with 100-year return period (in mm/hr)** As index 151 above, but for 100-year events.
- **157 24-hour total precipitation of events with 2-year return period (mm/day)**. As 151 but for 24-hour total precipitation sums. Sliding 24-hour windows, stepping at 1-hr resolution, are used.
- **158 24-hour total precipitation of events with 5-year return period (mm/day)** Sliding 24-hour windows, stepping at 1-hr resolution, are used.
- **159 24-hour total precipitation of events with 10-year return period (mm/day)**. Sliding 24-hour windows, stepping at 1-hr resolution, are used.
- **160 24-hour total precipitation of events with 20-year return period (mm/day)** Sliding 24-hour windows, stepping at 1-hr resolution, are used.
- **161 24-hour total precipitation of events with 50-year return period (mm/day)** Sliding 24-hour windows, stepping at 1-hr resolution, are used.
- **162 24-hour total precipitation of events with 100-year return period (mm/day)**. As 110 but for 24-hour total precipitation sums. Sliding 24-hour windows, stepping at 1-hr resolution, are used.
- **201 Mean sea level rise (cm)** has two components, i.e. IPCC based regional mean sea level rise and land uplift. The IPCC report provides the global mean sea level rise information, which was further downscaled to regional mean sea level rise for Denmark. The regional mean sea level rise is identical for the whole Denmark. The land uplift provides the difference for different coastal stretches.
- **202 Storm surge 20-year return events (cm)** is based on the 10 minutes sea level data from the HBM model output and observations.
- **203 Storm surge 50-year return events (cm)**. As 202 but for 50-year events.
- **204 Storm surge 100-year return events (cm)**. The historical period are based on KDI statistics and the future change only considers SLR.
- **205 Storm surge 10000-year return events (cm)**. As 204 but for 10000-year events.
- **206 Storm surge 1-year events (cm)**. As 202 but for 1-year events.
- **208 Storm surge 5-year events (cm)**. As 202 but for 5-year events.
- **210 Frequency of storm surge 20-year events (year)**. For the historical periods, it is calculated as the observation records divided by the number of events over 20-year return level. For the future periods, it is calculated as the simulations time (30 years) divided by the number of events over the historical 20-year return level.

- **301 Mean wind speed (m/s)**. Wind speed is calculated for bias-corrected data using the QQ-scaling method and given as a mean over a year or a season. Because of large gradients in wind speed inland from the coasts, the smoothing is reduced compared to other indices: a 25 x 25 km filter is applied instead of the general 75 x 75 km filter.
- **302 Extreme wind (m/s)** calculated as the number of days for a year or season with a maximum wind speed above 25 m/s.

  Because of large gradients in wind speed inland from the coasts, the smoothing is reduced compared to other indices: a 25 x 25 km filter is applied instead of the general 75 x 75 km filter.
- **401 Solar radiation (W/m^2)** Also know as 'globalstråling' in Danish; the sum of direct and diffuse sunlight reaching the surface. The corresponding model field is *downwelling shortwave radiation at the surface*.
- **402 Potential evaporation (mm/day)** Calculated using the Makkink formula based on temperature and solar radiation for both model and observational data.

RCP8.5	RCA4	CCLM	REMO	RACMO22E	HIRHAM5	WRF	ALADIN	RegCM	I alt
MOHC-HadGEM2-ES	1	1	1	1	1	2	1	1	9
ICHEC-EC-EARTH	3	2	1	3	3	1			13
CNRM-CERFACS-CNRM-CM5	1	1	1	1	1	1	1		7
NCC-NorESM1-M	1	1	1	1	1	1			6
MPI-M-MPI-ESM-LR	3	4	3	1	1	1		1	14
IPSL-IPSL-CM5A-MR	1			1		1			3
CCCma-CanESM2		1	1						2
MIROC-MIROC5		1	1			1			3
I alt	10	11	9	8	7	8	2	2	57
RCP4.5	RCA4	CCLM	REMO	RACMO22E	HIRHAM5	WRF	ALADIN	RegCM	I alt
MOHC-HadGEM2-ES	1	1		1	1				4
ICHEC-EC-EARTH	1	1		2	1				5
CNRM-CERFACS-CNRM-CM5	1	1		1			1		4
NCC-NorESM1-M					1				1
MPI-M-MPI-ESM-LR	1	1	2						4
IPSL-IPSL-CM5A-MR	1					1			2
I alt	5	4	2	4	3	1	1		20

Table 7: RCP8.5 (top) and RCP4.5 (bottom) EURO-CORDEX models used in producing the indexes 001, 101-106 and 108-109

RCP8.5	RCA4	CCLM	REMO	RACMO22E	HIRHAM5	WRF	ALADIN	RegCM	I alt
MOHC-HadGEM2-ES	1		1	1	1		1		5
ICHEC-EC-EARTH	3		1	1	3				8
CNRM-CERFACS-CNRM-CM5	1				1		1		3
NCC-NorESM1-M	1	1	1		1				4
MPI-M-MPI-ESM-LR	3	2	3		1			1	10
IPSL-IPSL-CM5A-MR	1								1
CCCma-CanESM2		1	1						2
MIROC-MIROC5		1	1						2
I alt	10	5	8	2	7		2	1	35
RCP4.5	RCA4	CCLM	REMO	RACMO22E	HIRHAM5	WRF	ALADIN	RegCM	I alt
MOHC-HadGEM2-ES	1			1	1				3
ICHEC-EC-EARTH	1			1	1				3
CNRM-CERFACS-CNRM-CM5	1						1		2
NCC-NorESM1-M					1				1
MPI-M-MPI-ESM-LR	1		2						3
IPSL-IPSL-CM5A-MR	1								1
I alt	5		2	2	3		1		13

Table 8: RCP8.5 (top) and RCP4.5 (bottom) EURO-CORDEX models used in producing the indexes 107, 151-162.

Table 9: Observational data used for the various climate indices. Data sources are labelled with numbers and are - **1:** Klimagrid Danmark (KGDK) from DMI database. A subset is available her: `https://www.dmi.dk/fileadmin/Rapporter/TR/tr12-10_20x20km.zip`. Note that KGDK precipitation data are not undercatch-corrected. - **2:** DMI database, Data-table on page 73 of Cappelen [2017] - **3:** Ditlevsen et al. [2019].

Number	Type of data	Source	Spatial res.	Time res.	Time coverage	Notes
001 - mean T	KGDK dataset	1	20×20km	Daily mean	1989–2019	Two files used, one for 1989-2000 and another for 2001-2019
002-005,007-009	KGDK dataset	1	10x10 km	Daily mean	2011-2019	-
101-106, 108, 109	KGDK dataset	1	10x10km	Daily mean	2004-2019	Daily files
107 - Cloudbursts	DMI hi-res precip network	2	≈ 258 stations	Minutes	2011-2016	Observed rate of cloud-bursts/year/station given station network
201 - 203 Ocean	KDI-based parameters	3	Coastal	Hourly - 10 min.	20th C - Now.	We use KDI-derived extreme-value distribution parameters for each station.
301 Wind	KGDK dataset	1	20x20 km	Daily mean	1989–2019	Two files used, one for 1989-2000 and another for 2001-2019
302 Wind	KGDK dataset	1	10x10 km	Daily mean	2011-2019	-
401 Globalstråling	KGDK dataset	1	20x20 km	Daily mean	1989–2019	Two files used, one for 1989-2000 and another for 2001-2019
402 Makkink evap.	KGDK dataset	1	20x20 km	Daily mean	1989–2019	Two files used, one for 1989-2000 and another for 2001-2019

Table 10: Standard deviations in climate indexes, based on bootstrapping of local anomaly data (i.e. excluding the enhanced variability otherwise due to inclusion of geographic variations). Observation year and models are bootstrapped – labelled S1 and S2. Two pieces of information is given for each index - one is the absolute value of an index in the far future period 2071-2100, and the other is the change in that index between the far future period and the historical reference period. These two quantities are shown in each column before and after the semi-colon. The changes are either absolute (indexes 001, 105, 106 and 107), or are given as percentages. Values shown are for the scenario RCP8.5 and the distributions generated by the bootstrap include the various values from each bootstrap across the whole 1x1 km land-only grid of Denmark. 9 bootstraps were performed. For each index two lines are shown - the first line gives the largest standard deviation found in any of the 10, 50 and 90%iles - the second line is restricted to just the 50%ile (i.e., the median). The seasonal and the annual values are all included, except for index 107, which is annual only.

#	**Name of index**	units	S1 (obs)	S2 (mod)
001	Mean temperature	$^{\circ}C : ^{\circ}C$	±0.18 : ±0.13 ±0.18 : ±0.13	±0.16 : ±0.17 ±0.12 : ±0.12
101	Mean precip.	mm/day : %	±0.13 : ±1.0 ±0.13 : ±0.9	±0.12 : ±5 ±0.09 : ±4
102	Daily-max precip.	mm : %	±1.7 : ±0.6 ±1.7 : ±0.5	±1.6 : ±6 ±1.0 : ±4
103	5-day max precip.	mm : %	±2.6 : ±0.86 ±2.5 : ±0.74	±2.0 : ±4 ±1.5 : ±3
104	14-day max precip.	mm : %	±3.9 : ±0.9 ±3.8 : ±0.8	±4.5 : ±5 ±2.4 : ±4
105	Days with over 10 mm Daily precip.	days : days	±0.7 : ±0.15 ±0.7 : ±0.13	±0.55 : ±0.57 ±0.43 : ±0.48
106	Days with over 20 mm Daily precip.	days : days	±0.35 : ±0.12 ±0.35 : ±0.10	±0.20 : ±0.20 ±0.14 : ±0.15
107	Number of cloud-bursts per year	events : events	- -	±0.074 : ±0.073 ±0.074 : ±0.073
151	Hourly precip. in 2-year events	mm : %	- -	±0.90 : ±7 ±0.69 : ±6
153	Hourly precip. in 10-year events	mm : %	- -	±3.0 : ±10 ±2.4 : ±9
156	Hourly precip. in 100-year events	mm : %	- -	±8.6 : ±16 ±5.9 : ±13
157	Daily precip. in 2-year events	mm : %	- -	±2.2 : ±5.3 ±1.7 : ±4.3
159	Daily precip. in 10-year events	mm : %	- -	±4.9 : ±7.8 ±3.0 : ±5.4
162	Daily precip. in 100-year events	mm : %	- -	±11.7 : ±11.4 ±5.8 : ±6.1
201	Mean sea level wrt. coastline		-	-
202	Storm surge 20-year events		-	-
203	Storm surge 50-year event		-	-

#	GCM	RCM	member	historical + rcp4.5 + rcp8.5 / historical + rcp8.5 / no data							
				tas	tasmax	tasmin	pr	pr1h	sfcWind	sfcWindmax	rsds
1	CANESM	CCLM	r1i1p1	h8	h8	h8	h8	h8	h8		h8
2	CANESM	REMO15	r1i1p1	h8	h8	h8	h8	h8	h8	h8	h8
3	CNRM	CCLM	r1i1p1	h48	h48	h48	h48		h48	h48	h48
4	CNRM	ALADIN	r1i1p1	h48	h48	h48	h48	h48	h48	h48	h48
5	CNRM	HIRHAM	r1i1p1	h8	h8	h8	h8	h8	h8	h8	h8
6	CNRM	RACMO	r1i1p1	h48	h48	h48	h48		h48	h48	h48
7	CNRM	RCA	r1i1p1	h48	h48	h48	h48	h48	h48	h48	h48
8	CNRM	REMO	r1i1p1	h8	h8	h8	h8		h8	h8	h8
9	CNRM	WRF381	r1i1p1	h8	h8	h8	h8		h8	h8	h8
10	ECEARTH	HIRHAM	r1i1p1	h8	h8	h8	h8	h8	h8	h8	h8
11	ECEARTH	RACMO	r1i1p1	h48	h48	h48	h48	h48	h48	h48	h48
12	ECEARTH	RCA	r1i1p1	h8	h8	h8	h8	h8	h8	h8	h8
13	ECEARTH	HIRHAM	r3i1p1	h48	h48	h48	h48	h48	h48	h48	h48
14	ECEARTH	RACMO	r3i1p1	h8	h8	h8	h8		h8	h8	h8
15	ECEARTH	RCA	r3i1p1	h8	h8	h8	h8	h8	h8	h8	h8
16	ECEARTH	CCLM	r12i1p1	h48	h48	h48	h48		h48	h48	h48
17	ECEARTH	HIRHAM	r12i1p1	h8	h8	h8	h8	h8	h8	h8	h8
18	ECEARTH	RACMO	r12i1p1	h48	h48	h48	h48		h48	h48	h48
19	ECEARTH	RCA	r12i1p1	h48	h48	h48	h48	h48	h48	h48	h48
20	ECEARTH	REMO15	r12i1p1	h8	h8	h8	h8	h8	h8	h8	h8
21	ECEARTH	WRF361	r12i1p1	h8	h8	h8	h8		h8		
22	ECEARTH	crCLIM	r12i1p1	h8	h8	h8	h8		h8	h8	h8
23	HADGEM	CCLM	r1i1p1	h48	h48	h48	h48		h48	h48	h48
24	HADGEM	HIRHAM	r1i1p1	h48	h48	h48	h48	h48	h48	h48	h48
25	HADGEM	RACMO	r1i1p1	h48	h48	h48	h48	h48	h48	h48	h48
26	HADGEM	RCA	r1i1p1	h48	h48	h48	h48	h48	h48	h48	h48
27	HADGEM	REMO15	r1i1p1	h8	h8	h8	h8	h8	h8	h8	h8
28	HADGEM	WRF361	r1i1p1	h8	h8	h8	h8		h8		h8
29	HADGEM	WRF381	r1i1p1	h8	h8	h8	h8		h8	h8	h8
30	HADGEM	ALADIN	r1i1p1	h8	h8	h8	h8	h8	h8	h8	h8
31	HADGEM	REGCM	r1i1p1	h8	h8	h8	h8		h8	h8	h8
32	IPSL	RACMO	r1i1p1	h8	h8	h8	h8		h8	h8	h8
33	IPSL	WRF381	r1i1p1	h48	h48	h48	h48		h48	h48	h48
34	IPSL	RCA	r1i1p1	h48	h48	h48	h48	h48	h48	h48	h48
35	MIROC	CCLM	r1i1p1	h8	h8	h8	h8	h8	h8		h8
36	MIROC	WRF361	r1i1p1	h8			h8		h8		h8
37	MIROC	REMO15	r1i1p1	h8	h8	h8	h8	h8	h8	h8	h8
38	MPI	CCLM	r1i1p1	h48	h48	h48	h48	h8	h48	h48	h48
39	MPI	HIRHAM	r1i1p1	h8	h8	h8	h8	h8	h8	h8	h8
40	MPI	RACMO	r1i1p1	h8	h8	h8	h8		h8	h8	h8
41	MPI	REGCM	r1i1p1	h8	h8	h8	h8	h8	h8	h8	h8
42	MPI	crCLIM	r1i1p1	h8	h8	h8	h8	h8	h8	h8	h8
43	MPI	crCLIM	r2i1p1	h8	h8	h8	h8		h8	h8	h8
44	MPI	crCLIM	r3i1p1	h8	h8	h8	h8		h8	h8	h8
45	MPI	RCA	r1i1p1	h48	h48	h48	h48	h48	h48	h48	h48
46	MPI	RCA	r2i1p1	h8	h8	h8	h8	h8	h8	h8	h8
47	MPI	RCA	r3i1p1	h8	h8	h8	h8	h8	h8	h8	h8
48	MPI	REMO09	r1i1p1	h48	h48	h48	h48	h48	h48	h48	h48
49	MPI	REMO09	r2i1p1	h48	h48	h48	h48	h48	h48	h48	h48
50	MPI	REMO09	r3i1p1	h8	h8	h8	h8	h8	h8	h8	h8
51	MPI	WRF361	r1i1p1	h8	h8	h8	h8		h8		h8
52	NORESM	HIRHAM	r1i1p1	h48	h48	h48	h48	h48	h48	h48	h48
53	NORESM	RACMO	r1i1p1	h8	h8	h8	h8		h8	h8	h8
54	NORESM	REMO15	r1i1p1	h8	h8	h8	h8	h8	h8	h8	h8
55	NORESM	RCA	r1i1p1	h8	h8	h8	h8	h8	h8	h8	h8
56	NORESM	WRF381	r1i1p1	h8	h8	h8	h8		h8	h8	h8
57	NORESM	crCLIM	r1i1p1	h8	h8	h8	h8	h8	h8	h8	h8

Figure 17: List of the 57 climate model simulations used for the v2020a and v2020b climate indices produced within Klimaatlas. Each row represents one model simulation with a forcing global climate model (GCM) and a downscaling regional climate model (RCM) and a member identification in the case when several downscalings are available. Each coloured column represents one variable used: tas (daily mean temperature), tasmax (daily maximum temperature), tasmin (daily minimum temperature), pr (daily total precipitation amount), pr1h (hourly total precipitation amount), sfcWind (daily mean wind speed), sfcWindmax (daily maximum wind speed) and rsds (daily mean downward shortwave radiation). Green colour data that are available for the historical period and both scenarios (RCP4.5 and RCP8.5). Yellow is shown when there are data for both the historical period and the RCP8.5 scenario. Red is shown when no data are currently available.

Acknowledgement
We acknowledge the World Climate Research Programme's Working Group on Regional Climate, and the Working Group on Coupled Modelling, former coordinating body of CORDEX and responsible panel for CMIP5. We also thank the climate modelling groups (listed in Tables 7 and 8 of this paper) for producing and making available their model output. We also acknowledge the Earth System Grid Federation infrastructure an international effort led by the U.S. Department of Energy's Program for Climate Model Diagnosis and Intercomparison, the European Network for Earth System Modelling and other partners in the Global Organisation for Earth System Science Portals (GO-ESSP)."

References

K. Arnbjerg-Nielsen. Quantification of climate change effects on extreme precipitation used for high resolution hydrologic design. *Urban Water Journal*, 9(2):57–65, April 2012. URL https://doi.org/10.1080/1573062x.2011.630091.

A. Arns, T. Wahl, I.D. Haigh, J. Jensen, and C. Pattiaratchi. Estimating extreme water level probabilities: A comparison of the direct methods and recommendations for best practise. *Coastal Engineering*, 81:51–66, November 2013. doi: 10.1016/j.coastaleng.2013.07.003. URL https://doi.org/10.1016/j.coastaleng.2013.07.003.

Jonathan L Bamber, Richard M Westaway, Ben Marzeion, and Bert Wouters. The land ice contribution to sea level during the satellite era. *Environmental Research Letters*, 13(6): 063008, jun 2018. ISSN 1748-9326. URL http://stacks.iop.org/1748-9326/13/i=6/a=063008?key=crossref.a29d19ff8e92d45a021c6aca08d2c874.

Jonathan L. Bamber, Michael Oppenheimer, Robert E. Kopp, Willy P. Aspinall, and Roger M. Cooke. Ice sheet contributions to future sea-level rise from structured expert judgment. *Proceedings of the National Academy of Sciences*, 116(23):11195–11200, May 2019. doi: 10.1073/pnas.1817205116. URL https://doi.org/10.1073/pnas.1817205116.

Per Berg and Jacob Weismann Poulsen. Implementation details for hbm. Technical Report 12-11, Danish Meteorological Institute, 2012. URL https://www.dmi.dk/fileadmin/Rapporter/TR/tr12-11.pdf.

T. A. Buishand. Extreme rainfall estimation by combining data from several sites. *Hydrological Sciences Journal*, 36(4):345–365, aug 1991. URL https://doi.org/10.1080/02626669109492519.

T.A. Buishand. Bivariate extreme-value data and the station-year method. *Journal of Hydrology*, 69(1-4):77–95, February 1984. URL https://doi.org/10.1016/0022-1694(84)90157-4.

John Cappelen. Ekstrem nedbør i danmark, opgørelser og analyser til og med 2016. Technical Report 17-06, Danish Meteorological Institute, 2017. URL https://www.dmi.dk/fileadmin/user_upload/Rapporter/TR/2017/DMIRep17-06.pdf.

John Cappelen. Ekstrem nedbør i danmark - opgørelser og analyser til og med 2018, tr19-06. Technical report, Danish Meteorological Institute, 2019. URL https://www.dmi.dk/fileadmin/user_upload/Rapporter/TR/2019/DMIRap19-06.pdf.

J. A. Church, P. U. Clark, A. Cazenave, J. M. Gregory, S. Jevrejeva, A. Levermann, M. A. Merrifield, G. A. Milne, R. S. Nerem, P. D. Nunn, A. J. Payne, W. T. Pfeffer, D. Stammer, and A. S. Unnikrishnan. Sea-level rise by 2100. *Science*, 342(6165):1445–1445, December 2013a. doi: 10.1126/science.342.6165.1445-a. URL https://doi.org/10.1126/science.342.6165.1445-a.

J.A. Church, P.U. Clark, A. Cazenave, J.M. Gregory, S. Jevrejeva, A. Levermann, M.A. Merrifield, G.A. Milne, R.S. Nerem, P.D. Nunn, A.J. Payne, W.T. Pfeffer, D. Stammer, and A.S. Unnikrishnan. *Sea Level Change*, book section 13, page 1137–1216. Cambridge University Press, Cambridge, United Kingdom and New York, NY, USA, 2013b. ISBN 978-1-107-66182-0. doi: 10.1017/CBO9781107415324.026. URL www.climatechange2013.org. *Editors: Stocker, T.F. and Qin, D. and Plattner, G.-K. and Tignor, M. and Allen, S.K. and Boschung, J. and Nauels, A. and Xia, Y. and Bex, V. and Midgley, P.M.*

Stuart Coles. *An Introduction to Statistical Modeling of Extreme Values*. Springer London, 2001. doi: https://doi.org/10.1007/978-1-4471-3675-0.

Sönke Dangendorf, Marta Marcos, Guy Wöppelmann, Clinton P. Conrad, Thomas Frederikse, and Riccardo Riva. Reassessment of 20th century global mean sea level rise. *Proceedings of the National Academy of Sciences*, 114(23):5946–5951, May 2017. doi: 10.1073/pnas.1616007114. URL https://doi.org/10.1073/pnas.1616007114.

Danmarks Statistik. Kvadratnet, 2019. URL https://www.dst.dk/da/TilSalg/produkter/geodata/kvadratnet.

Robert M. DeConto and David Pollard. Contribution of antarctica to past and future sea-level rise. *Nature*, 531(7596):591–597, March 2016. doi: 10.1038/nature17145. URL https://doi.org/10.1038/nature17145.

Charlotte Ditlevsen, Marta Ramos, Carlo Sørensen, Ulf Ciocan, and Thorsten Piontkowitz. Højvandsstatistikker 2017. Technical report, Kystdirektoratet, 2019. URL https://kyst.dk/media/80372/hoejvandsstatistikker2017revideret11022019.pdf.

M. G. Donat, G. C. Leckebusch, S. Wild, and U. Ulbrich. Future changes in european winter storm losses and extreme wind speeds inferred from GCM and RCM multi-model simulations. *Natural Hazards and Earth System Science*, 11(5):1351–1370, May 2011. doi: 10.5194/nhess-11-1351-2011. URL https://doi.org/10.5194/nhess-11-1351-2011.

Markus G Donat, Gregor C Leckebusch, Simon Wild, and Uwe Ulbrich. Benefits and limitations of regional multi-model ensembles for storm loss estimations. *Climate Research*, 44(2-3): 211–225, 2010. doi: 10.3354/cr00891. URL https://doi.org/10.3354/cr00891.

T Edwards, L Brandon, M A G Durand, and N R Edwards. Revisiting antarctic ice loss due to marine ice-cliff instability. *Nature*, 566(7742):58–64, 2019. doi: doi:10.1038/s41586-019-0901-4. URL https://doi.org/10.1038/s41586-019-0901-4.

W Fu, J She, and M Dobrynin. A 20-year reanalysis experiment in the Baltic Sea using three-dimensional variational (3DVAR) method. *Ocean Science*, 8(5):827–844, 2012. doi: 10.5194/os-8-827-2012.

I. B. Gregersen, H. Madsen, J.J. Linde, Krüger, and K. Arnbjerg-Nielsen. Opdaterede klimafaktorer og dimensionsgivende regnintensiteter Skrift nr. 30. Technical report, Spildevandskomiteen, 2014a.

I. B. Gregersen, M. Sunyer, H. Madsen, S. Funder, J. Luchner, and D. Ros. Past, present, and future variations of extreme precipitation in denmark. Technical report, Danish Technical University, 2014b.

Lonny Hansen. Sea level data 1889-2017 from 14 stations in denmark mean, maximum and minimum values calculated on monthly and yearly basis including plots of mean values. Technical Report 18-16, Danish Meteorological Institute, 2018. URL https://www.dmi.dk/fileadmin/Rapporter/2018/DMI_Report_18-16.pdf.

Carling C Hay, Eric Morrow, Robert E Kopp, and Jerry X Mitrovica. Probabilistic reanalysis of twentieth-century sea-level rise. *Nature*, 517(7535):481, 2015. doi: doi:10.1038/nature14093.

Simon J. Holgate, Andrew Matthews, Philip L. Woodworth, Lesley J. Rickards, Mark E. Tamisiea, Elizabeth Bradshaw, Peter R. Foden, Kathleen M. Gordon, Svetlana Jevrejeva, and Jeff Pugh. New data systems and products at the permanent service for mean sea level. *Journal of Coastal Research*, pages 493–504, 2013. doi: 10.2112/JCOASTRES-D-12-00175.1. URL https://doi.org/10.2112/JCOASTRES-D-12-00175.1.

J. R. M. Hosking, J. R. Wallis, and E. F. Wood. Estimation of the Generalized Extreme-Value Distribution by the Method of Probability-Weighted Moments. *Technometrics*, 27(3):251, August 1985. ISSN 00401706. URL http://www.jstor.org/stable/1269706?origin=crossref.

J. R.M. Hosking and J. R. Wallis. Parameter and quantile estimation for the generalized pareto distribution. *Technometrics*, 29(3):339–349, August 1987. URL https://doi.org/10.1080/00401706.1987.10488243.

Daniela Jacob, Juliane Petersen, Bastian Eggert, Antoinette Alias, Ole Bøssing Christensen, Laurens M. Bouwer, Alain Braun, Augustin Colette, Michel Déqué, Goran Georgievski, Elena

Georgopoulou, Andreas Gobiet, Laurent Menut, Grigory Nikulin, Andreas Haensler, Nils Hempelmann, Colin Jones, Klaus Keuler, Sari Kovats, Nico Kröner, Sven Kotlarski, Arne Kriegsmann, Eric Martin, Erik van Meijgaard, Christopher Moseley, Susanne Pfeifer, Swantje Preuschmann, Christine Radermacher, Kai Radtke, Diana Rechid, Mark Rounsevell, Patrick Samuelsson, Samuel Somot, Jean Francois Soussana, Claas Teichmann, Riccardo Valentini, Robert Vautard, Björn Weber, and Pascal Yiou. EURO-CORDEX: New high-resolution climate change projections for European impact research. *Regional Environmental Change*, 14(2):563–578, 2014. doi: 10.1007/s10113-013-0499-2.

M. Kallache, M. Vrac, P. Naveau, and P.-A. Michelangeli. Nonstationary probabilistic downscaling of extreme precipitation. *Journal of Geophysical Research*, 116(D5), March 2011. URL https://doi.org/10.1029/2010jd014892.

Eric M. Laflamme, Ernst Linder, and Yibin Pan. Statistical downscaling of regional climate model output to achieve projections of precipitation extremes. *Weather and Climate Extremes*, 12:15–23, June 2016. URL https://doi.org/10.1016/j.wace.2015.12.001.

A. N. Larsen, I. B. Gregersen, O. B. Christensen, J. J. Linde, and P. S. Mikkelsen. Potential future increase in extreme one-hour precipitation events over europe due to climate change. *Water Science and Technology*, 60(9):2205–2216, November 2009. URL https://doi.org/10.2166/wst.2009.650.

H. Madsen, I. B. Gregersen, D. Rosbjerg, and K. Arnbjerg-Nielsen. Regional frequency analysis of short duration rainfall extremes using gridded daily rainfall data as co-variate. *Water Science and Technology*, 75(8):1971–1981, February 2017. URL https://doi.org/10.2166/wst.2017.089.

Moritz Mathis, B Mayer, and Thomas Pohlmann. An uncoupled dynamical downscaling for the North Sea: method and evaluation. *Ocean Modelling*, 72:153–166, 2013. URL https://doi.org/10.1016/j.ocemod.2013.09.004.

Mathworks. The *scatteredInterpolant* routine, 2019. URL https://se.mathworks.com/help/matlab/ref/scatteredinterpolant.html.

Jerry X Mitrovica and Glenn A Milne. On post-glacial sea level: I. General theory. *Geophysical Journal International*, 154(2):253–267, 2003. URL https://doi.org/10.1046/j.1365-246X.2003.01942.x.

Jerry X Mitrovica, Natalya Gomez, and Peter U Clark. The sea-level fingerprint of West Antarctic collapse. *Science*, 323(5915):753–753, 2009. URL https://science.sciencemag.org/content/323/5915/753.

Jerry X Mitrovica, N Gomez, E Morrow, C Hay, K Latychev, and ME Tamisiea. On the robustness of predictions of sea level fingerprints. *Geophysical Journal International*, 187 (2):729–742, 2011. URL https://doi.org/10.1111/j.1365-246X.2011.05090.x.

MST. Miljøstyrelsen, 2019. URL https://mst.dk.

Sanne Muis, Martin Verlaan, Hessel C Winsemius, Jeroen CJH Aerts, and Philip J Ward. A global reanalysis of storm surges and extreme sea levels. *Nature communications*, 7:11969, 2016. URL https://doi.org/10.1038/ncomms11969.

Robert S Nerem, Brian D Beckley, John T Fasullo, Benjamin D Hamlington, Dallas Masters, and Gary T Mitchum. Climate-change–driven accelerated sea-level rise detected in the altimeter era. *Proceedings of the National Academy of Sciences*, 115(9):2022–2025, 2018. URL https://doi.org/10.1073/pnas.1717312115.

Martin Olesen, Kristine Skovgaard Madsen, Carsten Ankjær Ludwigsen, Fredrik Boberg, Tina Christensen, John Cappelen, Ole Bøssing Christensen, Katrine Krogh Andersen, and Jens Hesselbjerg Christensen. Fremtidige klimaforandringer i danmark. Technical Report 14-06, DMI, 2014. URL https://www.dmi.dk/fileadmin/user_upload/Rapporter/DKC/2014/Klimaforandringer_dmi.pdf.

M. Oppenheimer, Glavovic B., Hinkel J., R. van de Wal, A. Magen, A. Abd-Elgawad, R.S. Cai, M. Cifuentes-Jara, R.M. Deconto, T. Ghosh, J. Hay, F. Isla, B. Marzeion, B. Meyssignac, and Z. Sebesvari. *Sea Level Rise and Implications for Low Lying Islands, Coasts and Communities*, book 4. in press, 2019. URL www.ipcc.ch/srocc/download-report. Please be aware that this citation is the draft version, the final version will be available on the website after correction.

David T Pugh. *Tides, surges and mean sea level*. John Wiley and Sons Inc., New York, NY, 1987.

Madleine Samuelsson and Anders Stigebrandt. Main characteristics of the long-term sea level variability in the baltic sea. *Tellus A*, 48(5):672–683, 1996. doi: 10.1034/j.1600-0870.1996.t01-4-00006.x. URL https://onlinelibrary.wiley.com/doi/abs/10.1034/j.1600-0870.1996.t01-4-00006.x.

Mikael Scharling. Klimagrid - danmark nedbør, lufttemperatur og potentiel fordampning 20x20 & 40x40 km - metodebeskrivelse. Technical Report 99-12, Danish Meteorological Institute, 1999. URL https://www.dmi.dk/fileadmin/user_upload/Rapporter/TR/1999/tr99-12.pdf.

Mikael Scharling. Klimagrid Danmark nedbør 10x10 km (ver.2) - metodebeskrivelse. Technical Report 99-15, Danish Meteorological Institute, 2012. URL https://www.dmi.dk/fileadmin/user_upload/Rapporter/TR/1999/tr99-15.pdf.

SDFE. Styrelsen for dataforsyning og effektivisering, 2019. URL https://sdfe.dk/hent-data/datafordeleren/.

R Sibson. A brief description of natural neighbor interpolation. In V Barnett, editor, *Interpreting multivariate data*, pages 21–36. Wiley, Chichester, 1981.

Aimée BA Slangen, Benoit Meyssignac, Cecile Agosta, Nicolas Champollion, John A Church, Xavier Fettweis, Stefan RM Ligtenberg, Ben Marzeion, Angelique Melet, Matthew D Palmer, et al. Evaluating model simulations of twentieth-century sea level rise. Part I: global mean sea level change. *Journal of Climate*, 30(21):8539–8563, 2017. URL https://doi.org/10.1175/JCLI-D-17-0110.1.

Carlo Sørensen, H.T. Madsen, and S.B. Knudsen. Højvandsstatistikker 2012. Technical report, Kystdirektoratet, 2013.

Peter Riddersholm Wang and Mikael Scharling. Klimagrid danmark - dokumentation og validering af klimagrid danmark i 1x1 km opløsning. Technical Report 10-13, Danish Meteorological Institute, 2012. URL https://www.dmi.dk/fileadmin/Rapporter/TR/tr10-13.pdf.

Christopher S Watson, Neil J White, John A Church, Matt A King, Reed J Burgette, and Benoit Legresy. Unabated global mean sea-level rise over the satellite altimeter era. *Nature Climate Change*, 5(6):565–568, 2015. URL https://www.nature.com/articles/nclimate2635.

Philip L Woodworth, JR Hunter, Marta Marcos, P Caldwell, Margarita Menéndez, and I Haigh. Towards a global higher-frequency sea level dataset. *Geoscience Data Journal*, 3(2):50–59, 2016. URL https://doi.org/10.1002/gdj3.42.